

# Photometric Response Functions of the SDSS Imager

Mamoru Doi<sup>a,b</sup>, Masayuki Tanaka<sup>c</sup>, Masataka Fukugita<sup>b,d,e</sup>, James E. Gunn<sup>f</sup>, Naoki Yasuda<sup>b</sup>, Željko Ivezić<sup>g</sup>, Jon Brinkmann<sup>h</sup>, Ernst de Haars<sup>f</sup>, Scott J. Kleinman<sup>i</sup>, Jurek Krzesinski<sup>j</sup>, and R. French Leger<sup>h</sup>

<sup>a</sup>*Institute of Astronomy, University of Tokyo, Mitaka, Tokyo 1810015, Japan*

<sup>b</sup>*Institute for the Physics and Mathematics of the Universe, University of Tokyo, Kashiwa 2778582, Japan*

<sup>c</sup>*European Southern Observatory, Karl Schwarzschild Straße 2, Garching bei München 85748, Deutschland*

<sup>d</sup>*Institute for Advanced Study, Princeton, NJ08540, U. S. A.*

<sup>e</sup>*Institute for Cosmic Ray Research, University of Tokyo, Kashiwa 2778582, Japan*

<sup>f</sup>*Princeton University Observatory, Princeton, NJ 08540, U. S. A.*

<sup>g</sup>*Department of Astronomy, University of Washington, Box 351580, Seattle, WA 98195, U. S. A.*

<sup>h</sup>*Apache Point Observatory, @2001 Apache Point Road, P.O. Box 59, Sunspot, NM88349-0059, U. S. A.*

<sup>i</sup>*Gemini Observatory, 670 N. A'ohoku Place, Hilo Hawaii, 96720, U. S. A.*

<sup>j</sup>*Mt. Suhora Observatory, Cracow Pedagogical University, ul. Podchorazych 2, 30-084 Cracow, Poland*

## ABSTRACT

The monochromatic illumination system is constructed to carry out *in situ* measurements of the response function of the mosaicked CCD imager used in the Sloan Digital Sky Survey (SDSS). The system is outlined and the results of the measurements, mostly during the first 6 years of the SDSS, are described. We present the reference response functions for the five colour passbands derived from these measurements, and discuss column to column variations and variations in time, and also their effects on photometry. We also discuss the effect arising from various, slightly different response functions of the associated detector systems that were used to give SDSS photometry. We show that the calibration procedures of SDSS remove these variations reasonably well with the resulting final errors from variant response functions being unlikely to be larger than 0.01 mag for  $g$ ,  $r$ ,  $i$ , and  $z$  bands over the entire duration of the survey. The considerable aging effect is uncovered in the  $u$  band, the response function showing a 30% decrease in the throughput in the short wavelength side during the survey years, which potentially causes a systematic error in photometry. The aging effect is consistent with variation of the instrumental sensitivity in  $u$ -band, which is calibrated out. The expected colour variation is consistent with measured colour variation in the catalog of repeated photometry. The colour variation is  $\Delta(u - g) \sim 0.01$  for most stars, and at most  $\Delta(u - g) \sim 0.02$  mag for those with extreme colours. We verified in the final catalogue that no systematic variations in excess of 0.01 mag are detected in the photometry which can be ascribed to aging and/or seasonal effects except for the secular  $u - g$  colour variation for stars with extreme colours.

## 1. Introduction

A unique and unprecedented feature of the Sloan Digital Sky Survey (SDSS: York et al. 2000) is the wide field CCD imager (Gunn et al. 1998) that enables us to image 1.52 square degrees (the physical

area size is  $725 \text{ cm}^2$ ) of the sky at a time. The prime concern is the accurate characterisation of the imaging efficiency across the five colour passbands of the SDSS. For this purpose we have constructed a monochromatic illumination system and installed it permanently in the imager enclosure. We have carried out detection efficiency measurements several times during the SDSS operation. This enables us to study the variation of the response function over the survey period. We have then compared photometry with the designed and/or measured characteristics of the imager in the laboratory, and with photometry of the associated telescopes with SDSS filters to qualify SDSS photometry.

This paper describes the monochromatic illumination system and the detector efficiency measurement, and presents the response function for the SDSS main imager which is used as the reference. We discuss the effect that is expected on SDSS photometry from seasonal, secular and chip to chip variations of the response efficiency, and compare it with the actual data acquired by the survey after the routine photometric calibration. We also study response functions of the associated telescopes used in photometric calibrations for SDSS and study the effect on SDSS photometry from their slightly variant system responses. We believe that this helps us understand SDSS photometry better as well as serves as a useful guide for designing comparable systems in the instrumentation planned in the future.

The photometric system comprises five colour bands,  $u$ ,  $g$ ,  $r$ ,  $i$ , and  $z$ , that divide the entire range from the atmospheric ultraviolet cutoff at  $3000 \text{ \AA}$  to the sensitivity limit of silicon CCDs at  $11000 \text{ \AA}$  into five non-overlapping passbands, maximising the band width of each band to enhance the detection efficiency (Fukugita et al. 1996, hereinafter F96). The blue side of the  $g$ ,  $r$  and  $i$  passbands is cut off by colloidal colour glass elements (GG400, OG550 and RG695, respectively) and their red side by short-pass interference multilayer (30–45 layers) coatings made of  $\text{TiO}_2$  and  $\text{SiO}_2$ . The characteristics of the  $u$  filter is determined by ionically coloured glass, BG38 and UG11, for the blue and red sides, respectively, while an interference coating made of  $\text{Ta}_2\text{O}_5$  and  $\text{SiO}_2$  is applied to suppress the redleak that would otherwise appear at  $6600\text{--}8000\text{\AA}$ . For the  $z$  passband, the blue side is cut off by colloidal colour glass RG830, and the red side is open, naturally cut off by the silicon CCDs.

CCD detectors for the main imager are thinned back-illuminated devices except for those for the  $z$  band which use thick front-illuminated devices, all procured from Scientific Imaging Technologies, Inc (SITE). An ultraviolet-enhancing antireflection coating was applied to the CCDs used for the  $u$  band. The filters, directly cemented on the second quartz corrector of the Richey-Chrétien telescope, are placed just before the CCDs. The containers that house the filters and CCDs are vacuumised all the time for the duration of the survey except for necessary maintenance periods. The CCD that is used at the 50-cm Photometric Telescope (hereafter PT), which has been used to set the zero point of photometry and to monitor atmospheric extinction, and the CCD at the USNO 1m telescope system, which was used to preset brightness of standard stars, are also UV-enhancing coated, thinned back-illuminated devices similar to the  $u$  CCDs in the main camera.

We have measured the transmission of filters in the laboratory before their installation to the imager. The transmission was verified to be sufficiently close to the design, allowing for some variation in the cutoff wavelength up to  $10\text{--}20\text{\AA}$  that arise from fluctuations in the commercially available colour glass elements (Schott, Mainz) and different batches of coatings (Asahi Spectra Co., Tokyo). The response of the CCD was measured at SITE but only at a room temperature. This curve was then modified at long wavelengths to fit the data obtained at operating temperature (about  $-80\text{C}$ ) in our laboratory, using, however, coarsely sampled measurements. Synthesized response curves for the specific device used for PT were published in F96, which defines the original photometric system of SDSS. The response curves used for the survey with the 2.5m telescope camera, therefore, are expected

to differ by some extent from the one that defines the SDSS photometric system. The camera itself has six assemblies (called Camcols) of 5 detectors, one for each colour (hence 30 CCD's and filters), and the six individual systems are, of course, not exactly the same as each other.

We also anticipated that the system response may be subject to some seasonal variation (the CCDs are cooled, but the filters run approximately at the ambient temperature of the telescope enclosure) and possibly to aging effects. We have designed and constructed a monochromatic illumination system to characterize the wavelength response of all of the camera CCDs/filters, and have occasionally measured the system response during the duration of the survey to monitor the seasonal and secular effects.

After we began the operation of the 2.5m telescope (Gunn et al. 2006) we found that the response functions deviated significantly due to an effect that was completely unexpected in the beginning. The filters are in vacuum, with the coated surface exposed. In vacuum, water molecules, which have been adsorbed into the voids in the relatively low-density evaporated films used in the filters, migrate away, lowering the refractive index of the films and moving the cutoff wavelength of the  $g$ ,  $r$ , and  $i$  filters blueward by about a 2.3 percent (120Å, 160Å, and 175Å, respectively). The same effect would also modify the redleak suppression of the  $u$  filters. Laboratory measurements of this effect, motivated by the early measurements of the imager using the illumination system, are reported in Fukugita & Shimasaku (2009) (hereafter FS09). The result of our early measurement was given in Fan et al. (2001).

The preparation for the calibration work has been somewhat patchy, due to a pressing time schedule when the survey began and to a number of problems that surfaced in the early stage of observations. The basic system was defined in F96 for the combination of the filters and the CCD that were supposed to be used for the Photometric Telescope, originally intended to be used both to define magnitudes of the standard stars and to carry out the photometric calibration for the 2.5m telescope, together with a daily monitor of atmospheric extinction. However, due to technical problems and a subsequent delay in installing the PT (called the Monitor Telescope at that time) photometry of the standard stars was actually carried out using the system at the USNO 1m telescope in Flagstaff with a set of filters that were slightly different, due to manufacturing variations, from those for PT. The zero points for the USNO system were adjusted to the F subdwarf spectrophotometric standard BD+17°4708 in the PT system, as given by F96.

The 50cm Photometric Telescope eventually installed at Apache Point Observatory (APO) has observed both standard stars, whose magnitudes were adopted from observations at USNO, and stars in secondary patches which were simultaneously measured by the 2.5m main telescope and thus used as transfer fields. The brightness of stars in the secondary patches was measured with respect to the USNO brightness for the set of standard stars that define the zero point of SDSS photometry (Smith et al. 2002; Tucker et al. 2006), originally denoted as primed magnitudes (FS96). Further complications were caused by the fact that the set of filters used at PT was replaced in the middle of the survey (18 August 2001, Modified Julian Date (hereafter MJD) 52140) with a new set which was fabricated using a more modern technique of ion-assisted deposition coating. This is forced by the fact that we discovered that the old filters made with traditional evaporated coatings display changes with temperature and humidity, smaller than the changes observed going to a fully evacuated environment, but still substantial. These changes are almost certainly associated again with the adsorption of water in the low-density evaporated films. The ion-assisted films are much denser and do not show the effects, as we also confirmed in laboratory experiments. The filters with evaporation-deposition films show a temperature dependence in excess of what was anticipated from the temperature dependence

of colour glass<sup>1</sup>. In vacuo, as in the 2.5m imager, the evaporated films show *no temperature* effects, however.

This instability was also noted by Tucker et al. (2006) during their work on photometric standard stars at the PT, who attempted to remove the effect by using variable color terms (‘b-terms’) so as not to affect the final results. The determination of these transformations and tracking them in time, however, is difficult and results in somewhat ambiguous photometric results. We thus decided to replace the PT filter set with a new one made with ion-assisted deposition coating, which makes the filter characteristics stable against environmental conditions. We designed the transmission of PT filters to fall between the one in vacuo and the one in air so that it can be close to the PT system in the dry air-purged environment with which some amount of the work had already been done.

We thus have used several systems that have somewhat different response functions to set up SDSS photometry. It is, therefore, important to examine that all relevant photometric response functions are sufficiently close to each other so that the resulting photometry defines a system at least with tolerable internal errors. This compels us to measure the response functions of PT (before and after the filter replacement), USNO and all 30 devices of the 2.5m telescope imager, in addition to that used to define the original photometric system. We note that the fiducial response functions of the 2.5m telescope imager have been made public through the world wide web at the SDSS site (SDSS public web site 2001)<sup>2</sup> using our measurements in December 2000. In this paper we present the newly estimated response function based on the entire measurements, but primarily resorting to those measured in the autumn of 2004 with more careful wavelength calibrations. The response function for the *u* band we shall present is significantly different from the one made public because of an unexpected large aging effect, but the other reference response functions we present differ little from the ones in the public web site. Even with the response functions as much varied as in the *u* band, the effects on calibrated photometry in the SDSS output turn out to be tolerably small. We note in passing that though we will do all our calculations as if the SDSS photometry is an AB system, we will not address the very difficult problem of determining the AB zero-point corrections, which could well be as large as a few hundredth of a magnitude.

In Section 2 we present the design of the monochromatic illumination system. In section 3 we present the results of the response function measurements, and present the new reference response function constructed therefrom. In section 4 we consider the effects expected from the variation of response functions on photometry. We also discuss the response function of associated telescopes used to give SDSS photometry and errors in photometry when these slightly different systems are used. We also study the actual data, which are published in SDSS catalogues (Abazajian et al. 2003; 2004; 2005; Adelman-McCarthy et al. 2006; 2007; 2008) after processing and calibrations by the photometric pipelines with the aid of the monitor telescope pipeline (Stoughton et al. 2002; Tucker et al. 2006).

---

<sup>1</sup> The red cutoff wavelength shifted by an unexpected amount, 42Å for *g*, 58Å for *r* and 77Å for *i* redwards when temperature increases by 20 deg (FS09). They are about 5 times worse than the temperature dependence for the colour glass used for the blue side cutoff. These shifts were much more than anticipated and would cause a few hundredth of magnitude shift. As mentioned in the text above, a very dry condition would affect the coating surface and hence the character of transmission. The filter at PT is purged with very dry air. It is so dry that the transmission of filters has shifted halfway between the air and the vacuum. We realised that it is difficult to control the exact condition; this forced us to decide that we replace the filters with ones made with the new technique. We confirmed that this effect together with the temperature dependence disappears with filters fabricated by the ion-assisted deposition coating technique.

<sup>2</sup> <http://www.sdss.org/dr7/instruments/imager/filters/u.dat,...z.dat>

## 2. Monochromatic illumination system

The illumination system consists basically of a lamp, a monochromator consisting of a grating, order sorting filters and slits, an integrating sphere and a photodiode to measure the flux of the illumination. This system can be moved accurately over the focal plane to illuminate any CCD in the camera, and also to illuminate a calibrated reference diode. The output of the integrating sphere is a few inches above the quartz corrector element which also serves as the mechanical substrate upon which the imager dewars are mounted, about 10 inches above the focal plane (Gunn et al. 1998). The X direction (the direction across different camera columns for the same colour band) is controlled by a ball-screw stepping motor, while the Y direction (the direction across five different colour filters in a single dewar) is manually controlled. Thus six CCDs with a given colour band can be reached by remote control, but measuring different colour bands requires manual intervention. Since the (manual) slit width must sometimes be changed when going from one colour band to another anyway, this is not onerous. The illumination covers 250 nm to 1200 nm with the resolution  $R = \lambda/\Delta\lambda = 50 - 200$  for a 0.5–2 mm slit width. The lamp is a Philips quartz-halogen tungsten-filament lamp of 150W with the filament size 3mm×5mm. The flux is 5000 lm and the colour temperature is 3400K at 24 V. Its life time, 50 hours at 24 V, is increased to 500 hours when run at 20 V, at which voltage the colour temperature is 3200K.

The light is condensed with a mirror system, and is then guided to a slit of the monochromator with adjustable width 1-20 mm by a triangular mask. The monochromator (JASCO CT-10) consists of four mirrors which make a collimated beam with a diameter of about 30 mm. The mirror focal length is 100 mm, with an approximate focal ratio of F/3. A grating of 28 mm×28 mm with 1200 lines/mm is used to disperse the light with the spectral dispersion about 6.7 nm/mm at 600 nm. The grating is controlled by a stepping motor. The beam is guided through the outlet slit, whose width is set equal to that of the input slit, to the order-sorting filter, consisting of three filters, U-330 for 250–390 nm, L-37 for 390–680 nm and R-64 for 680–1200 nm. The output light illuminates an integrating sphere (ORIEL) 8 inches in diameter, and a shutter is placed before the integrating sphere. The integrating sphere makes the illumination over the surface of a CCD as uniform as we can. The output is through a circular hole of 2 inches in diameter. The illuminating hole is placed vertically so that distance to CCD mimics the F/5 beam of the telescope. A 61.7mm thick aluminium block with a cylindrical hole of 2.5 inch diameter is attached at the illuminating hole, which works as a light guide. The inside of the cylinder is anodised so that it works as a light baffle. Figure 1 shows the entire unit.

The light flux is monitored by a photodiode (Hamamatsu Photonics, S2281) whose detection efficiency is accurately known. The sensitivity of the photodiode was measured by Hamamatsu Photonics from 200 to 1080 nm at a 10 – 20 nm interval. We may obtain the idea about the error of the sensitivity by replacing the photodiode with alternative photodiode, which leads us to convince that it is no more than  $\approx 0.5\%$ . The absolute sensitivity of the photodiode is verified by Japan Quality Assurance Organisation, showing that the accuracy is better than 0.6 – 0.7% at 488.0 nm and at 835.1 nm. This photodiode is placed at the baffle of the cylinder hole of the block beneath the integration sphere. This is used to monitor the illumination flux, i.e., the efficiency of the CCD including the filter transmission is measured relative to the flux received at this photodiode.

The photodiode signals are converted into voltage with an AD743 operational amplifier, and data acquisition is done with National Instruments DAQ-700 at 1000 data points per exposure. The illumination apparatus and the photodiode data acquisition are controlled with National Instruments PCMCIA-GPIB. The entire measurement sequences are programmed and controlled by a LINUX computer in the SDSS control room, except for changing the manual stage positions, choosing a slit

width and a lamp voltage.

The parameters of the monochromator are set as follows: the slit width is 0.5 mm for *g*, *r*, and *i*-band, 0.75 mm for *u*-band, and 1.0 mm for *z*-band. which corresponds to the spectral resolution of 5.6 nm, 3.6 nm, 3.3 nm, 3.0nm, and 5.5 nm for *u*, *g*, *r*, *i*, and *z*-band respectively. The QTH lamp works at 20.0 Volt for *g*, *r*, *i*, and *z*-band, and 22.5 Volt for *u*-band. The exposure time is 2 sec to 100 sec depending on the efficiency of the passband at the wavelength being measured so that the CCD output is 3,000 – 30,000 electrons per pixel. Typical errors of repeated measurements were found to be less than  $\sim 0.5\%$  in efficiency.

We were not prepared to measure accurately the absolute detection efficiency at each measurement. We occasionally placed another photodiode at the distance the same as that to CCD to estimate the absolute detection efficiency. The absolute normalisation of the detection efficiency we quote in the next section is obtained from such measurements, unless otherwise stated. We expect systematic errors of the order no worse than 10% in the absolute normalisation, which is mainly due to geometrical uncertainty of the hardware setting. Relative efficiency was estimated with the photodiode placed at the integrating sphere. We scaled each measurement to that with the absolute measurement by adjusting it with an appropriate normalization factor.

Another important issue is the wavelength calibration. We measured the wavelength of the monochromatic illumination repeatedly with a portable fibre spectrometer, Asahi Spectra HSU-100S, which was calibrated against lines of a Hg+Ar lamp for the range 250–1000 nm. As a whole we estimate that the wavelength accuracy of the monochromatic illumination is kept to an error less than  $\pm 3\text{\AA}$ , at least for the measurements with wavelength calibration carried out in July 2004 and after. In earlier measurements we did not use the portable spectrometer and the monochromator was directly calibrated with  $H\alpha$  and  $H\beta$  emissions from a hydrogen lamp; the position of lamp could not be accurately controlled and was likely somewhat different from the original one for the quartz-halogen lamp and hence the wavelength calibration was not as accurate as it was with later measurements. In this report we correct early measurements using ones measured after July 2004 by matching the red side cutoff, whose wavelength has been sufficiently stable in the vacuum chamber.

We note that the deviations of the incident angle of the light from exactly perpendicular causes a shift of cutoff wavelengths of interference filter, as

$$\Delta\lambda = \sqrt{1 - c_i \sin^2 \theta} \quad (1)$$

where  $c_i = 0.62, 0.57, 0.58$  for *g*, *r*, and *i* filters;  $\theta$  is the angle from perpendicular. This gives  $\approx 0.2\%$  in the wavelength, or 8–12 $\text{\AA}$  depending on the passband for  $\theta = 4$  deg, corresponding approximately to the average over an F/5 beam with the secondary obscuration. Hence the real transmission of the red-side cutoff in *g*, *r*, and *i* band may systematically be shorter by 8–12  $\text{\AA}$  than with the parallel beam. Our illumination system produces an F/5 beam, however, without the secondary obscuration which gives  $\approx 0.1\%$  (4–6  $\text{\AA}$ ) shifts. Hence, we still expect 4–6  $\text{\AA}$  shift for the red cutoff in *g*, *r*, and *i* band responses. This effect is not large, and is wavelength dependent within each band pass. We do not correct for this effect in the present work, but include this into systematic errors.

The illumination of the monochromator covers roughly the whole size of the CCD, on which the flux varies only by  $< 8\%$ . Some fringing pattern is visible in the red end of the *i* band illumination, but it is at most 2%, and the effect can be small enough when an average is taken over some extended pixels. We set a region with the circular aperture of 100 pixel radius near the centre for our measurements. The repeated measurements with exposures using the same setting give the median counts that agree within 0.5%. (They are however mostly due to small flux variation of the QTH lamp, and are mostly

absorbed when compared against the flux at the photodiode.)

Along with the measurement of the response functions, we occasionally measured gains of the detectors. A few pairs of the same exposures were taken with the same set up of the monochrometer as the response function measurement, and the images were subtracted between the two and the standard deviations in counts were measured. The input fluxes in counts and the deviations then give the detector gain. The raw data for the response functions derived above were multiplied by the gains to obtain the quantum efficiency.

Figure 2 shows an example of the measurement of the quantum efficiency of a UV-enhancing coated thinned CCD without a filter, the specific device used for the Photometric Telescope. The solid points are obtained with the present monochrometer illumination system with the CCD cooled to operating temperature and the open points represent the data which were measured at SITE at room temperature but were warped to trace the broadband measurements at a working temperature in our laboratory for the same CCD. We see agreement between the two at 1–2% accuracy, although the measurement in the UV is somewhat noisy. The latter is the curve we used in the characterisation of the SDSS response function in F96.

### 3. The measurement

We have carried out measurements at 11 epochs before 2006 (and one in 2008); the journal is given in Table 1. The measurement is time consuming, and full measurements were not done at all the epochs, because of time constraints. The results are summarised in Fig. 3 (u), Fig. 4 (g), Fig. 5 (r), Fig. 6 (i) and Fig. 7 (z). The response functions for the 2.5m telescope main imager that we will take as the reference are shown by thick solid curves. They are obtained by averaging our measurements over 6 columns of detectors, obtained in October and November 2004, as described below. When some measurements for specific columns are missing we supplement the data from other measurements, after applying a correction for temperature effects. In order to take into account the reflection losses due to the primary and the secondary mirrors of the telescope, we included reflection losses from two fresh aluminium surfaces, which modify the efficiencies by 20–30 percent while change the shapes of the curves only slightly. The attenuation due to the first corrector lens is significantly smaller than 1% at all the wavelengths, and hence it is not included in our analysis. The monochromator measurements presented in this paper include the attenuation due to the secondary corrector.

The thin solid curves indicate the response function that has been taken as the standard from the beginning of the survey as described in F96. It was obtained by the synthesis of the measured transmission and the quantum efficiency of the relevant filters and CCD. These specific filters and CCD have been used at PT before the filter replacement. The curves also include reflection of two aluminium surfaces. This represents the response functions for PT with the original filter set, allowing, however, for variations caused by environmental effects.

There are two more curves drawn. The thin dashed curves are synthesised response functions expected for the USNO 1m telescope system. Since the actual quantum efficiency was not measured for the CCD used in the USNO system, the quantum efficiency of the PT CCD was used, for the USNO system uses a CCD with surface treatment identical to that used at PT. The other curves, drawn dotted, are the response functions for the PT with the new set of filters.

For the *u* band (Figure 3) a large departure of the reference response function for the 2.5m telescope imager from the others is apparent at shorter wavelengths  $\lambda < 3650\text{\AA}$ . This is ascribed to

the aging effect we will discuss below.

Another conspicuous set of deviations of the 2.5m reference response curves is seen around the red edges with the  $g, r$  and  $i$  bands. We see that the red edges of the 2.5m reference response curves are significantly blueward of the other curves. This shift is caused by coating films placed in the vacuum environment, as mentioned earlier. The shifts amount to 120 ( $g$ ), 160 ( $r$ ) and 175Å ( $i$ ), which are also confirmed in laboratory experiments (FS09). Some variations up to  $(40 - 50)$ Å are also seen at the blue edges, which are mostly due to fluctuations of characteristics of colour glass, and to a minor extent to the temperature effect which we shall discuss below. Similar differences visible at red edges between the F96 standard and USNO are fluctuations in coatings. The temperature effect is absent for the red edge. The curves for the PT (with newer filters) falls between the F96 standard and the 2.5m reference curves (except for the  $g$  band which lies somewhat outside the F96 standard, as a result of fluctuations in the coating process): this is as designed when we made the new set of filters for PT.

Interference coatings from different coating batches lead to some fluctuations in the cutoff wavelengths up to 30-40Å, which are within our specifications given to the vendor. Interference films even in the same batch of coating may also vary to the extent up to 15Å due to inhomogeneity in the coating vessel. The transmission of coloured glass also shows fluctuations of the same order from piece to piece. We did not reject the filters unless the effective wavelengths differ substantially more than by 30Å from the specification.

For the  $z$  band (Figure 7) the large difference between the 2.5m reference response curve and the others is due to the lower quantum efficiency of the front-illuminated thick CCDs in the main imager, compared with thinned CCD used for the other curves. This causes an appreciable difference in the effective wavelengths.

As a quantitative measure for the variation of response functions we use the effective wavelength or the effective frequency defined by

$$\begin{aligned} \lambda_{\text{eff}} &= c/\nu_{\text{eff}}, \\ \nu_{\text{eff}} &= \frac{\int \nu R(\nu) d\nu / h\nu}{\int R(\nu) d\nu / h\nu}, \end{aligned} \quad (2)$$

where  $R(\nu)$  is the response function and the integrand is weighted to give the photon number<sup>3</sup>. Note that this definition of effective frequency  $\nu_{\text{eff}}$  differs from the one used in Table 2 of F96, where  $1/h\nu$  is not included. This definition is the average with respect to the photon *number*, not energy, which is the relevant quantity for nearly all modern detectors, CCDs included. Table 2 also gives the effective wavelengths  $\lambda_{\text{eff}}$  and the wavelengths at the 50% yield of the maximum at both blue and red edges for four response functions (without atmospheric transmission) shown in Fig. 3–7. The PT system before the replacement of filters is the F96 standard, ignoring temperature effects. Note that the shape of the response function is modified by atmospheric extinction in actual observations, while we work with the intrinsic response function without atmospheric extinction in laboratories, and hence in this paper up to some exceptions when we refer to the observation, for which we include the effect due to atmospheric extinction.

The response curves should vary from column to column even within the main imager, although the interference film transmission varies less, because all film coatings used for the main imager are

---

<sup>3</sup>There are several definitions for effective wavelengths. The traditionally used is  $\int \lambda d\lambda / \int d\lambda$  for photomultiplier measurements. For other definitions, see F96

made in one single batch for each colour. Figure 8 (a)–(e) shows the response curve for each column of the imager for the five colour bands to show the column to column variation. These data are taken from the measurement in October/November 2004. The difference of  $\lambda_{\text{eff}}$  relative to the 2.5m reference measured at 3 epochs is presented in Table 3, the dispersions being  $8.9\text{\AA}$  for  $u$ ,  $5.8\text{\AA}$  for  $g$ ,  $6.5\text{\AA}$  for  $r$ ,  $4.1\text{\AA}$  for  $i$ ,  $27.5\text{\AA}$  for  $z$ . The larger variations for the  $z$  band are due to different CCD sensitivities near the red cutoff. We saw a very small variation ( $0.8\text{\AA}$ ) in the transmission curve of  $z$  filters used for the main imager in the measurement when the filters are produced. For other colours the dispersions of the difference are consistent with those of the filters we measured at the time of procurement, except for the  $u$  band for which *in situ* measurements in combination with CCD give a larger dispersion if only by a factor of two. Observed in the measurement is approximately what is anticipated for  $g$ ,  $r$  and  $i$ . The maximum deviation of  $\lambda_{\text{eff}}$  against the reference is  $(+9, -16)\text{\AA}$  for  $u$ ,  $(+6, -15)\text{\AA}$  for  $g$ ,  $(+4, -16)\text{\AA}$  for  $r$ ,  $(+6, -6)\text{\AA}$  for  $i$  and  $(+46, -31)\text{\AA}$  for  $z$ .

Figures 9(a)–(e) show the results of our measurements for the  $u - z$  bands at specified columns and Figure 9 (f) is for redleak of the  $u$  filter at Camcol 1 on April 2000, December 2000, September 2001, July 2004, October/November 2004 and December 2006. The 2.5m reference is also drawn for comparison. Measurements for other columns give similar results. The most conspicuous variation at different epochs is visible for the  $u$  band as we have already noted above (Figure 9(a)). The response functions, notably at shorter wave lengths, diminish as time passes till July 2004: the sensitivity diminished by  $\sim 30\%$  between the year 2000 and 2004. The characteristics has gradually stabilised, so that such a large variation was not visible after July 2004. We confirmed that no appreciable aging effects are visible with the  $u$  filters at the PT and the spare  $u$  filters retained at the laboratory. We also noticed that the illumination pattern visible on the CCD chip in our measurement in 2004 differs from the one in earlier measurements for the  $u$  band. No such conspicuous aging effects are visible in other colour bands. These observations lead us to suspect that aging is basically due to that of the sensitivity of the ultraviolet sensitive CCD itself, probably the deterioration of the ultraviolet enhancing coating and/or the associated manipulation of the surface potential profiles on the devices.

The time variations of the response curves in other passbands are small. We have shown in Figure 10 the time dependence of the effective wavelengths and the cut-off wavelengths as a function of the epoch of the measurement. Except for the  $u$  filters the time variation of  $\lambda_{\text{eff}}$  is of the order of  $\lesssim 10\text{\AA}$ , which is mostly seasonal. For instance, we observe the average difference  $4.2 \pm 2.5\text{\AA}$  between July 2004 and November 2004 for the  $g$  band. We made careful wavelength calibration work in the operations of July and November 2004. So we focus on the two measurements. This seasonal variation is largely ascribed to the temperature effect of GG400 colour glass used to cut off the blue side. The air temperature decreases by 17 deg between the two epochs. The measured shift of the blue edge  $6.8 \pm 1.3\text{\AA}$  is consistent with  $7.2\text{\AA}$  expected from the laboratory experiment for the temperature effect on GG400<sup>4</sup>. The red side cutoff varies little,  $1.8 \pm 1.6\text{\AA}$ , which is consistent with null within the error. The red side cutoff wavelengths of interference coating films such as those on the new PT

---

<sup>4</sup>The Schott document gives the temperature coefficient  $0.7\text{\AA}/\text{deg}$  for GG400 between 10–90 deg C, but our measurement in the laboratory (FS09) for this glass piece gives  $0.43/\text{deg}$  at -10–20 deg C, the temperature variation being smaller than the Schott value by a factor of 2. We noted that the temperature dependence is not quite linear. We found that the temperature dependence is mild at low temperatures and it becomes sharper at higher temperatures. The observed wavelength shift is consistent with our laboratory measurement. Similarly, we get  $0.75\text{\AA}/\text{deg}$  for OG530 compared with the Schott value of  $1.3\text{\AA}/\text{deg}$ , and  $0.55\text{\AA}/\text{deg}$  for RG695 compared with the Schott value of  $1.8\text{\AA}/\text{deg}$ . For RG830 our  $1.1\text{\AA}/\text{deg}$  is compared with  $2.3\text{\AA}/\text{deg}$  by Schott. The  $u$  filters are cut by colour glasses for both sides: BG38 (and UG11) for the blue side and UG11 for the red side. The temperature dependence is  $0.5\text{\AA}/\text{deg}$  at the laboratory, while the numbers are not given in the Schott catalogue. Unlike the coating surface, this does not depend on whether the environment is air or vacuum (FS09)

filters made with ion-assisted deposition are stable against temperature, which we have confirmed in laboratory experiments (FS09).

Similarly, we find a shift of  $14.7 \pm 0.5 \text{ \AA}$  in the blue edge of the  $r$  passband as compared with  $12.8 \text{ \AA}$  expected from the temperature dependence measurement for colour glass pieces. The same trend also applies to the  $i$  filter. The shift in the blue edge is measured to be  $21.0 \pm 0.8 \text{ \AA}$  for the  $i$  filter, as compared with  $9.2 \text{ \AA}$  ( $35 \text{ \AA}$  if the Schott catalogue value is used) expected from our laboratory experiments. The measured shifts of the red edge cutoff are  $2.0 \pm 0.8 \text{ \AA}$ ,  $-2.0 \pm 0.8 \text{ \AA}$  for the  $r$  and  $i$  passbands, respectively, which are again consistent with null shifts when the systematic error of  $3 \text{ \AA}$  in the wavelength calibration is taken into account. The temperature dependence is not clearly identified for the  $u$  passband in our measurements. For the  $z$  filter the measured blue edge shift  $51 \pm 21 \text{ \AA}$  appears larger than those expected from the temperature dependence of a laboratory measurement  $19 \text{ \AA}$ , but is consistent with the Schott value  $40 \text{ \AA}$ . In summary, the effective wavelength shift of the filter is grossly consistent with the temperature dependence of the colour glass cutoff. This change is smaller than  $\sim 20 \text{ \AA}$  for the  $u$  to  $i$  bands, small enough to cause any significant effects on photometry at a 1% level, as we will see in the next section. This is also true with the  $z$  band, although the shift itself is larger.

The  $z$  band response function curves appear to show the time variation in their shapes. We infer that the variation is due to the variation of the operational temperature of the CCD, which may have not been controlled well. We know that the quantum efficiency is sensitive to the temperature in reddest wavelengths.

We remark that the accuracy of our earlier measurements was somewhat lower: the sampling pitch in early measurements is too coarse for an accurate characterisation of the response function; a careful wavelength calibration is made only after July 2004; positional control of the illumination system could not be done very accurately in the beginning, etc. The measurements were significantly better controlled in the 2004 and later runs. We show in Table 5 summary of various uncertainties in the effective wavelength.

Figure 9 (f) presents the redleak measurement for the  $u$  response function for Camcol 1. The  $u$  filter composed of UG11 (1 mm) and BG38 (1 mm) colour glass causes redleak between  $6600 \text{ \AA}$  to  $8000 \text{ \AA}$ , which is suppressed by interference coating. Our best design of coating still produces a small red leak at around  $7900\text{--}8100 \text{ \AA}$  with an amplitude of  $\sim 5 \times 10^{-4}$ . In the figure, sharp peaks are seen at around  $7700\text{--}7800 \text{ \AA}$  in the amount of  $\sim 4 \times 10^{-4}$  (we subtract the floor of the peak as discussed in what follows). The  $100 \text{ \AA}$  redward shift of the interference coating compared with the design is caused by the vacuum environment. This would degrades the suppression; we were concerned about this, but we found that the redleak suppression is actually still sufficiently strong. We also observe another bump at  $6800\text{--}7500 \text{ \AA}$ . Our laboratory measurements for the  $u$  filters show that the suppression in this wavelength range is strong enough and does not exhibit any evidence for the leak in this region. We suspect from the wavelength interval that this leakage signal might be produced by a cross talk and scattered light that goes through the  $i$  filter ( $6800\text{--}8200 \text{ \AA}$ ) which is placed in the row next to the  $u$  filter. This interpretation also accounts for the shoulder seen in the red wing of the  $u$  filter leak at around  $\sim 8000 \text{ \AA}$ . We interpret this to be due to scattered light in the measurement and, hence, a fake, so that this floor is subtracted to estimate the redleak for  $u$  filters. Redleak depends on the filter. We detect the peak at about  $7670 \text{ \AA}$  for Camcol 2, 5 and 6 and  $7830 \text{ \AA}$  for Camcol 3 and 4 as shown in Figure 11. We have not seen the aging and/or seasonal effects in the  $u$ -band redleak more than 10% (Fig.9(f)).

This in turn indicates the order of magnitude of the effect of the scattered light and shows that it is small enough and does not affect the measurement for the main band pass.

For most purposes, we want to work with one representative response function for the 2.5m Telescope imager for the entire duration of the survey observations. We take the measurement of October–November 2004, for which we have nearly complete data sets (one measurement for *r1* is missing, and we adopt the data from measurement at other times and correct for the empirically known temperature effect). The season is between summer and winter, at temperatures close to the mean over the operation. This response function was that shown in Figure 3–7 above, with numerics given in Table 4<sup>5</sup>. The reflectivity for two fresh aluminium surfaces in the telescope is multiplied. These data are used to calculate  $\lambda_{\text{eff}}$  in Table 2 above. For the *u* band response function we include a representative redleak that is obtained by averaging over the column to column variation. The floor which is likely to be ascribed to scattered light is removed as seen in Figure 11. The atmospheric transmission at 1.3 airmass which we use in this work is also shown in the last column of Table 4. Here the transmission at the Palomar Observatory (altitude 1700m) is converted to the one at the APO (altitude 2788m) assuming the exponential scale height of the atmosphere of 7000m.

#### 4. Effects on photometry

We discuss the effects expected on photometry due to the small differences in response functions from column to column and from their variations with the epoch during the survey. We also consider the difference in photometry due to the use of different response functions among the 2.5m telescope main imager, Photometric Telescope, and the USNO detector system. Comparisons with the original F96 standard are also made. The SDSS primary standard stars (Smith et al. 2002) were observed using the USNO system, and then those observations are tied to the 2.5-m system with the Photometric Telescope. Our results confirm that the colour effects between two systems are sufficiently small.

Let us consider brightness of the fundamental standard star, F subdwarf BD+17°4708 (Oke 1990), by a synthetic analysis. The AB magnitude is defined by

$$m = -2.5 \log \frac{\int d(\log \nu) f(\nu) R(\nu)}{\int d(\log \nu) R(\nu)} - 48.60 \quad (3)$$

with  $f(\nu)$  the object flux. The flux of F subdwarf BD+17°4708 calculated with the various response function is given in magnitude in Table 6. Note that the photometric system used in F96 (and also in the present paper) is AB<sub>95</sub>, which differs slightly from the AB<sub>79</sub> system used by Oke & Gunn (1983)<sup>6</sup>. The numbers in the bottom row is the flux that would be obtained with the use of the response functions presented in the SDSS web site (SDSS public web site 2001). We note that the survey adopts the system normalised to the response function expected at 1.3 airmasses of atmospheric extinction, so that the atmospheric effect that modifies the response function must be included in  $R(\nu)$  when one discusses the actual observation (while the atmospheric attenuation of the flux is removed). The fluxes (in magnitude) that would be obtained in various detection systems with 1.3 airmass response functions for BD+17°4708 are presented in Table 7. They differ from the numbers in Table 6 by smaller than 0.01 mag except for the *u* passband for which the difference amounts to about 0.036–0.039 mag due to a large atmospheric effect. The effective wavelengths for this case are also given in upper rows in this table.

---

<sup>5</sup>Tables for each column are available from <http://www.ioa.s.u-tokyo.ac.jp/~doi/sdss/SDSSresponse.html>

<sup>6</sup>If one uses the AB<sub>79</sub> Vega spectrum, the brightness of BD+17°4708 for the F96 responses will be  $u = 10.498$ ,  $g = 9.631$ ,  $r = 9.329$ ,  $i = 9.219$  and  $z = 9.194$ . These differ from the numbers given in Table 6 (AB<sub>95</sub>) which are about 0.030–0.038 mag fainter. If one adopts the spectrum by Bohlin & Gilliland (2004), the brightness of BD+17°4708 for the F96 responses will be  $u = 10.563$ ,  $g = 9.616$ ,  $r = 9.343$ ,  $i = 9.254$  and  $z = 9.247$ .

In practice, in the application to SDSS photometry all measured fluxes are adjusted to fit the standard scale adopted from F96, and the variations seen in this table are absorbed into the calibration. In Table 7 we see that the difference among the different systems is at most 0.038 mag ( $u$  band). In  $g$  and  $r$  it is 0.034 mag and 0.007 mag respectively, and even smaller for redder colour bands. This change would cause constant shifts in photometry, so that relative magnitudes will be unchanged. These variations, however, are flattened by the calibration process when the fluxes are presented in the catalogue. We emphasise that the fluxes in Table 7 are not yet intended to give accurate AB magnitudes taken as the standard, but are referred to here for the purpose of comparisons among different systems.

The flux defined by eq. (3) depends primarily on  $\lambda_{\text{eff}}$ , and the change of the sensitivity tends to cancel between the numerator and the denominator. We find that the  $\lambda_{\text{eff}}$  dependence is roughly  $\delta m_u \simeq -0.105\Delta\lambda_{\text{eff}}/(100\text{\AA})$ ,  $\delta m_g \simeq -0.077\Delta\lambda_{\text{eff}}/(100\text{\AA})$ ,  $\delta m_r \simeq -0.044\Delta\lambda_{\text{eff}}/(100\text{\AA})$ ,  $\delta m_i \simeq -0.032\Delta\lambda_{\text{eff}}/(100\text{\AA})$ ,  $\delta m_z \simeq -0.024\Delta\lambda_{\text{eff}}/(100\text{\AA})$ , where  $\Delta\lambda_{\text{eff}}$  is the change in the effective wavelength between the two systems considered, for the BD+17°4708 spectrum.

The values presented in Table 6 and 7 ignore redleaks of the  $u$  filters. The contribution depends much on colour of stars. For stars with  $g - r < 0.6$  it is smaller than  $-0.01$  mag, but increases to  $-0.05$  mag for  $g - r \approx 1$ , and it can be as large as  $-0.5$  mag for very red stars such as  $g - r \approx 1.6$ . Therefore caution is necessary when one deals with red stars.

The time variations of the main imager are shown in the lowest two panels of Figure 10 (they are shown column by column). The panels (v) represent brightness of BD+17°4708 with 1.3 airmass atmosphere. In order to show the time-dependent variation of the sensitivity, we also show in panel (iv) the CCD output,  $\sim -2.5 \log N_{p.e.}$ , i.e., eq.(3) where the denominator is replaced by unity, so that it represents the variation of the number of photoelectrons in CCD (using the response function without atmosphere). With the brightness definition this variation is largely cancelled by the denominator in eq.(3): brightness of objects (magnitude) is sensitive solely to the shift of the effective wavelength. The decline of the CCD sensitivity in the  $u$  band seen in Fig. 10 (iv) is as much as 30% (or  $\approx 0.3$  mag; somewhat smaller if 1.3 airmass atmosphere is excised), which agrees with the size we expect from the change of the response function seen in Fig. 9 (a). This is reduced to a  $-0.03$  mag (in the opposite sign) change in magnitude if the brightness definition is used (Fig. 10 (v)), and such a variation should further be reduced by calibration procedures. For other colour bands, the change of the sensitivity is 0.01 mag for  $g$  and  $r$ , and 0.03 mag for  $i$  and  $z$ . These variations are also largely cancelled by the denominator in eq.(3), and the variation in brightness is smaller than 0.01 mag, which could in principle be further reduced by calibration procedures. Note that the numbers given here are colour dependent and apply only to BD+17°4708. The calibration would reduce these variations by enforcing measured brightness to the SDSS reference magnitudes obtained at USNO. When one is interested in sub-percent accuracy photometry, separate treatments of Camcols are desired (Ivezić et al. 2007).

Similar considerations apply to colours. Each detector has a slightly different response function, which causes some tilts in colour space. We estimate the magnitude difference at the column  $A$  of the camera relative to the 2.5m reference  $\Delta m_A = m_A - m_{\text{ref}}$  as a function of colour in Figure 12 for the five colours, where the stars used are taken from the spectrophotometric atlas by Gunn & Stryker (1983). The variation is largest in the  $u$  and  $z$  bands. It can be as much as 0.02 magnitudes, especially for red stars. The variation is also fairly large for  $g_2$  (and  $r_3$ ). For others it is mostly smaller than 0.01 mag. We see that  $\Delta m$  nearly vanishes for  $g - r \simeq -0.5$  for  $g$ , and for  $g - r \sim 0$  for  $r$  and  $i$ . These variations are without calibration and are reduced by photometric calibrations.

We then consider the difference of colours that depends on associated telescope systems used. Figure 13-15 shows the colour-colour plot written in the form  $\Delta(j - k)_{AB} = (j - k)_{\text{system A}} - (j - k)_{\text{system B}}$  as a function of  $(j - k)_{\text{standard}}$  to enhance the scale of the difference which is tiny. Here,  $j, k$  stand for  $u, g, r, i$ , and  $A$  and  $B$  are two different systems. Again, Gunn-Stryker’s spectrophotometric atlas is used for the sample. This represents the bare system-dependent colour term of each system. Figure 13 is the colour term of the USNO system against the F96 original standard, Figure 14 is that of PT against USNO, and Figure 15 is the 2.5m telescope imager (reference) against the USNO. Note that colour measured with PT, and hence with the 2.5m telescope imager, is adjusted to that with the USNO system for some set of standard stars in the calibration procedure (Smith et al. 2002; Tucker et al. 2006). The output of the 2.5m telescope is calibrated with stars measured by PT in secondary patches which are calibrated with some sets of the standard stars, which are given fixed values throughout all observations, and therefore variations are, in principle, largely cancelled by this reset. The SDSS photometry is published after these calibrations against secondary standard stars.

To verify that the variations we have seen here have not directly propagated into the final SDSS output photometry catalogues, we show in Figure 16(a) and (b) the time variation of  $r$  and  $u$  magnitudes of stars in the SDSS catalogue in a patch of 2.5 deg square (R.A.=5°, dec=0°) taken from Stripe 82 from the epoch July 1999 to January 2004. The difference from the mean is calculated for 600 stars with  $r < 18$  for  $r$  and 200 stars with  $u < 18.5$  for  $u$  by tracing photometry in time taken from Data Release 6 Supplement. The error bars indicate the variance in the sample. We see that both  $r$  and  $u$  magnitudes are very stable, the variation being less than 0.01 mag. In particular, the large variation expected for the  $u$  band sensitivity ( $\Delta u \simeq 0.3$  mag) between year 2000 and 2004 does not appear in Figure 16(b). We confirmed that this is also true with brightness in other colour bands.

To differentiate the aging effect possibly seen in the  $u$  band, we consider the variation of  $u - g$  colour, as a function of  $g - i$  colour. Most of the variation in the  $u$  band is absorbed into a time-varying constant adjusted in the calibration, but the colour effect is suspected to remain in the final catalogue, since the photometric calibrations do not take account of the colour term. The time variation in  $u - g$  colours seen in photometry of stars at stripe 82 (Ivezić et al. 2007) is plotted in Figure 17. The figure shows the mean differences of  $u - g$  measured in the first four years of the survey (1998 – 2002) and the later four years (2004 – 2007) as a function of  $g - i$  colour. We note that it is so adjusted in the calibration that  $\Delta(u - g)$  is zero as a matter of principle for stars of normal colour, which are used to determine the zero points in  $u$  and  $g$ .  $\Delta(u - g)$  is about -0.01 mag for blue stars ( $g - i \sim -0.2$ ) and is about -0.01mag for red stars ( $g - i \sim 2$ ). This difference can be larger, as much as -0.02 mag, for extremely red stars (we note that  $g - r \approx (g - i)/1.2$ ). This is compared with the plot (shown by crosses) that shows the expected variation using spectral synthesis of Gunn-Stryker stars between 2001 and 2004. We conclude that photometry is consistent with what is expected from the secular variation of the response function, although the variation is small, of the order of 0.01 mag except for extreme colours. We expect a larger change for very blue stars, but we have no appropriate sample of such stars in our data base. We confirmed that the variation was no more than 0.005mag for  $g - r, r - i$ , and  $i - z$ .

Another way to find the instrumental variation in observational data, e.g., such as variations due to aging of the  $u$  band detectors, may be to look at the nightly calibration monitor data for the so called a-term, the difference in the nightly zero point between the atmospheric extinction corrected instrumental magnitude and the magnitude taken as the standard (Tucker et al. 2006). This may directly measure the sensitivity of the system. Figures 18(a) and (b) show this term as a function of the epoch of observations. In the  $u$  band (Figure 18(b)), we observe a rapid change as much as 0.4 mag from MJD51000 (5 July 1998) to MJD52200 (6 November 2001), and a gradual decline then to

MJD 53200 (13 July 2004). The trend and size are consistent with what is anticipated from the aging effect. We also observe some change in the  $r$  band (Figure 18 (a)), to at most 0.1 mag, the reason of which is not clearly identified.

## 5. Summary

We have described the *in situ* measurement of the response functions of the SDSS 2.5 telescope imager, which has been used to produce the SDSS astronomical catalogues during the period of 2000 to 2007. We then discussed the effect of variations of the response function on photometry. We also presented the outline of the monochromatic illumination system constructed for this purpose.

We studied the variation of the response functions from column to column and also in time over the duration of the survey, both secularly (aging) and with environmental temperature. We presented the reference response function of the 2.5m telescope imager as a mean over the 6 columns of the imager. We showed the detection of a significant aging effect for the  $u$  band, especially in the short wavelength side, which amounts to about a 30 percent decrease in the sensitivity over the period of the survey.

We confirmed, however, that brightness appears to be invariable to 0.01 mag over the years, and the SDSS catalogues is likely to be accurate to this level: we confirmed that the error caused by variations of the response function is not a dominant component of the error in photometry. Time variability was also detected for the response function for other colour bands, but it is small and well within our tolerable errors. The variation other than that for the  $u$  passband is ascribed mostly to the temperature dependence of transmission properties of the colour glass that composes the filters.

We have studied the seasonal, secular and column to column variations of the response function and their effects on photometry. We also studied the effect of the use of the associated systems that have slightly different response functions in the SDSS photometric calibration procedure. We have verified that the effect of the variation of the response function, which may amount to 0.01 mag in  $g$ ,  $r$ ,  $i$  and  $z$  bands and, and variations among 6 different devices of the imager, which also amount to 0.01–0.02 mag, are cancelled very well by calibration procedures and do not appear in the final SDSS catalogues; the residual effects are not larger than 0.01 mag for all passbands. We have expected sizable aging effects in the response function for the  $u$  band, but photometric calibrations absorbs most of variations and the variation visible in the SDSS catalogue is small.

The variation of  $u - g$  colours is of the order of  $\Delta(u - g) \sim 0.01$  mag except for stars with extreme colours for which it can be 0.02 mag.

## Acknowledgement

We thank Kazuhiro Shimasaku for his work for filter experiments to characterise environmental effects, carried out with one of the present authors (MF). We are grateful to Maki Sekiguchi for his advice in the construction of the monochromatic illumination system, and Jeff Pier for his arrangement that allowed our work to characterise the USNO 1m detector system. We thank Advanced Technology Centre of NAOJ at which our laboratory filter measurements were carried out. We also thank Michael A. Carr, Brian R. Elms, George A. Pauls, Robert H. Lupton, Constance M. Rockosi, Craig Loomis, James Annis, Daniel C. Long, and Shannon Watters for their helps in installation and operation of the monochromator at APO. We thank Tanner Nakagawara for his preliminary analysis of catalogued

data. We also thank John Marriner, Naotaka Suzuki, and an anonymous referee for their very useful comments. MF is supported by the Friends of the Institute at Princeton, and received Grant in Aid of the Ministry of Education (Japan) at Tokyo. MD and NY are also supported by Grants in Aid of the Ministry of Education (Japan) and by a JSPS core-to-core program, International Research Network for Dark Energy. MD and ŽI would like to thank the Aspen Center for Physics for their kind support to carry out a part of this work.

Funding for the SDSS and SDSS-II has been provided by the Alfred P. Sloan Foundation, the Participating Institutions, the National Science Foundation, the U.S. Department of Energy, the National Aeronautics and Space Administration, the Japanese Monbukagakusho, the Max Planck Society, and the Higher Education Funding Council for England. The SDSS Web Site is <http://www.sdss.org/>.

The SDSS is managed by the Astrophysical Research Consortium for the Participating Institutions. The Participating Institutions are the American Museum of Natural History, Astrophysical Institute Potsdam, University of Basel, University of Cambridge, Case Western Reserve University, University of Chicago, Drexel University, Fermilab, the Institute for Advanced Study, the Japan Participation Group, Johns Hopkins University, the Joint Institute for Nuclear Astrophysics, the Kavli Institute for Particle Astrophysics and Cosmology, the Korean Scientist Group, the Chinese Academy of Sciences (LAMOST), Los Alamos National Laboratory, the Max-Planck-Institute for Astronomy (MPIA), the Max-Planck-Institute for Astrophysics (MPA), New Mexico State University, Ohio State University, University of Pittsburgh, University of Portsmouth, Princeton University, the United States Naval Observatory, and the University of Washington.

## REFERENCES

- Abazajian, K., et al. 2003, *AJ*, 126, 2081
- Abazajian, K., et al. 2004, *AJ*, 128, 502
- Abazajian, K., et al. 2005, *AJ*, 129, 1755
- Adelman-McCarthy, J. K., et al. 2006, *ApJS*, 162, 38
- Adelman-McCarthy, J. K., et al. 2007, *ApJS*, 172, 634
- Adelman-McCarthy, J. K., et al. 2008, *ApJS*, 175, 297
- Bohlin, R. C. & Gilliland, R. L. 2004, *AJ*, 128, 3053
- Fan, X., et al. 2001, *AJ*, 121, 31
- Fukugita, M., Ichikawa, T., Gunn, J. E., Doi, M., Shimasaku, K., & Schneider, D. P. 1996, *AJ*, 111, 1748
- Fukugita, M. & Shimasaku, K., in preparation
- Gunn, J. E., et al. 1998, *AJ*, 116, 3040
- Gunn, J. E., et al. 2006, *AJ*, 131, 2332
- Gunn, J. E., & Stryker, L. L. 1983, *ApJS*, 52, 121
- Ivezić, Ž., et al. 2007, *AJ*, 134, 973

Oke, J. B. 1990, AJ, 99, 1621

Oke, J. B., & Gunn, J. E. 1983, ApJ, 266, 713

Smith, J. A., et al. 2002, AJ, 123, 2121

Stoughton, C., et al. 2002, AJ, 123, 485

Tucker, D. L., et al. 2006, Astronomische Nachrichten, 327, 821

York, D. G., et al. 2000, AJ, 120, 1579

Table 1: Journal of response function measurements. The number stands for measured Camcol.

Date	$u$	$g$	$r$	$i$	$z$
Jan. 2000	6	1	4	1	2-4,6
Apr. 2000	1	1	1,4	1	1-2
Dec. 2000	1-6	1-6	1-6	1-6	1-6
Sep. 2001		1-2	1-2	1-6	
Jul. 2004	1-2	1-6	1-4	1-3	1-2
Oct. 2004	1-5				
Nov. 2004	6	1-6	2-6	1-6	1-6
May 2005	2-4		1		
Jul. 2005	2		1		
Sep. 2006	5-6				
Dec. 2006	1-6		1-6		
May 2008	1-6	1-6	1-6	1-6	1-6

Table 2: Filter characteristics <sup>a</sup>

system	$\lambda_{\text{eff}}(u)$	$\lambda_{\text{blue}}(u)$	$\lambda_{\text{red}}(u)$	$\lambda_{\text{eff}}(g)$	$\lambda_{\text{blue}}(g)$	$\lambda_{\text{red}}(g)$	$\lambda_{\text{eff}}(r)$	$\lambda_{\text{blue}}(r)$	$\lambda_{\text{red}}(r)$	$\lambda_{\text{eff}}(i)$	$\lambda_{\text{blue}}(i)$	$\lambda_{\text{red}}(i)$	$\lambda_{\text{eff}}(z)$	$\lambda_{\text{blue}}(z)$	$\lambda_{\text{red}}(z)$
F96 standard	3499	3216	3849	4728	4076	5485	6200	5548	6934	7615	6939	8474	9054	8334	9741
PT-new	3496	3207	3838	4714	4035	5506	6180	5559	6879	7593	6971	8346	9054	8334	9741
USNO	3500	3211	3847	4704	4057	5476	6201	5551	6930	7606	6931	8461	9051	8329	9739
2.5m reference	3531	3259	3852	4627	4019	5330	6140	5589	6748	7467	6902	8178	8887	8257	9347
SDSS “public”	3498	3203	3844	4627	4022	5330	6139	5593	6748	7467	6903	8171	8927	8271	9449

<sup>a</sup>  $\lambda_{\text{eff}}$  is defined in eq. (2) in the text,  $\lambda_{\text{blue}}$  and  $\lambda_{\text{red}}$  are defined as the wavelengths that give 50% of the peak response function. PT-new is the PT system after the filter replacement. The system before the filter replacement is the same as F96 standard. SDSS “public” means the response function that is made public through the world wide web (2001). All characteristics are without atmosphere transmissions.

Table 3: Measured  $\lambda_{\text{eff}}$  differences from the 2.5m reference case in Å.

epoch	column	$\lambda_{\text{eff}}(u)$	$\lambda_{\text{eff}}(g)$	$\lambda_{\text{eff}}(r)$	$\lambda_{\text{eff}}(i)$	$\lambda_{\text{eff}}(z)$
2.5m reference		3531	4627	6140	7467	8887
2000 Dec.	1	−40	−8	+0	−8	+23
	2	−43	−18	+3	+5	+89
	3	−30	−1	−19	+6	+57
	4	−28	−2	+1	+0	+50
	5	−37	+4	−10	−2	+16
	6	−34	+1	+1	−5	−2
2004 Jul.	1	+7	−1	+16	+8	+20
	2	+7	−11	+14	+19	+77
	3	—	+10	−8	+19	—
	4	—	+8	+11	—	—
	5	—	+9	—	—	—
	6	—	+9	—	—	—
2004 Oct./Nov.	1	−2	−5	—	−6	−17
	2	−5	−15	+4	+5	+46
	3	+9	+6	−16	+6	+9
	4	−7	+4	+2	−1	+19
	5	−16	+4	+0	−2	−14
	6	+5	+5	+2	−6	−31

Table 4. 2.5m telescope reference response function and adopted atmospheric transmission for APO  
(airmass = 1.3)

$\lambda$	$u$	$g$	$r$	$i$	$z$	$T_{1.3airmass}$
2940	0.0001	—	—	—	—	0.0162
2960	0.0003	—	—	—	—	0.0242
2980	0.0005	—	—	—	—	0.0351
3000	0.0009	—	—	—	—	0.0459
3020	0.0014	—	—	—	—	0.0644
3040	0.0029	—	—	—	—	0.0828
3060	0.0050	—	—	—	—	0.1048
3080	0.0077	—	—	—	—	0.1303
3100	0.0136	—	—	—	—	0.1558
3120	0.0194	—	—	—	—	0.1882
3140	0.0276	—	—	—	—	0.2206
3160	0.0367	—	—	—	—	0.2628
3180	0.0460	—	—	—	—	0.2962
3200	0.0558	—	—	—	—	0.3269
3220	0.0656	—	—	—	—	0.3521
3240	0.0743	—	—	—	—	0.3728
3260	0.0826	—	—	—	—	0.3912
3280	0.0905	—	—	—	—	0.4067
3300	0.0969	—	—	—	—	0.4224
3320	0.1033	—	—	—	—	0.4369
3340	0.1098	—	—	—	—	0.4496
3360	0.1162	—	—	—	—	0.4608
3380	0.1223	—	—	—	—	0.4687
3400	0.1268	—	—	—	—	0.4766
3420	0.1314	—	—	—	—	0.4824
3440	0.1353	—	—	—	—	0.4882
3460	0.1390	—	—	—	—	0.4977
3480	0.1427	—	—	—	—	0.5109
3500	0.1460	—	—	—	—	0.5241
3520	0.1494	—	—	—	—	0.5311
3540	0.1518	—	—	—	—	0.5382
3560	0.1537	—	—	—	—	0.5452
3580	0.1555	—	—	—	—	0.5522
3600	0.1570	—	—	—	—	0.5593
3620	0.1586	0.0002	—	—	—	0.5660
3640	0.1604	0.0015	—	—	—	0.5728
3660	0.1625	0.0027	—	—	—	0.5795
3680	0.1638	0.0038	—	—	—	0.5862
3700	0.1626	0.0035	—	—	—	0.5930
3720	0.1614	0.0032	—	—	—	0.5979
3740	0.1563	0.0031	—	—	—	0.6027
3760	0.1497	0.0037	—	—	—	0.6076
3780	0.1416	0.0048	—	—	—	0.6125
3800	0.1282	0.0067	—	—	—	0.6174
3820	0.1148	0.0115	—	—	—	0.6231
3840	0.0956	0.0220	—	—	—	0.6289
3860	0.0744	0.0353	—	—	—	0.6346
3880	0.0549	0.0507	—	—	—	0.6404
3900	0.0407	0.0740	—	—	—	0.6461
3920	0.0265	0.0973	—	—	—	0.6534
3940	0.0177	0.1224	—	—	—	0.6606
3960	0.0107	0.1484	—	—	—	0.6679
3980	0.0050	0.1757	—	—	—	0.6751
4000	0.0032	0.2081	—	—	—	0.6824

Table 4—Continued

$\lambda$	$u$	$g$	$r$	$i$	$z$	$T_{1.3airmass}$
4020	0.0015	0.2404	—	—	—	0.6876
4040	0.0008	0.2617	—	—	—	0.6928
4060	0.0005	0.2785	—	—	—	0.6981
4080	0.0003	0.2954	—	—	—	0.7033
4100	0.0003	0.3122	—	—	—	0.7086
4120	0.0003	0.3290	—	—	—	0.7129
4140	0.0002	0.3411	—	—	—	0.7172
4160	0.0001	0.3512	—	—	—	0.7215
4180	—	0.3603	—	—	—	0.7258
4200	—	0.3660	—	—	—	0.7301
4220	—	0.3717	—	—	—	0.7339
4240	—	0.3773	—	—	—	0.7378
4260	—	0.3830	—	—	—	0.7416
4280	—	0.3886	—	—	—	0.7455
4300	—	0.3943	—	—	—	0.7493
4320	—	0.3999	—	—	—	0.7529
4340	—	0.4043	—	—	—	0.7564
4360	—	0.4083	—	—	—	0.7600
4380	—	0.4122	—	—	—	0.7635
4400	—	0.4161	—	—	—	0.7671
4420	—	0.4200	—	—	—	0.7705
4440	—	0.4240	—	—	—	0.7739
4460	—	0.4279	—	—	—	0.7773
4480	—	0.4314	—	—	—	0.7808
4500	—	0.4337	—	—	—	0.7842
4520	—	0.4359	—	—	—	0.7873
4540	—	0.4381	—	—	—	0.7904
4560	—	0.4404	—	—	—	0.7935
4580	—	0.4426	—	—	—	0.7965
4600	—	0.4448	—	—	—	0.7996
4620	—	0.4470	—	—	—	0.8021
4640	—	0.4488	—	—	—	0.8047
4660	—	0.4504	—	—	—	0.8072
4680	—	0.4521	—	—	—	0.8097
4700	—	0.4537	—	—	—	0.8122
4720	—	0.4553	—	—	—	0.8141
4740	—	0.4569	—	—	—	0.8160
4760	—	0.4586	—	—	—	0.8179
4780	—	0.4601	—	—	—	0.8199
4800	—	0.4611	—	—	—	0.8218
4820	—	0.4622	—	—	—	0.8237
4840	—	0.4633	—	—	—	0.8256
4860	—	0.4644	—	—	—	0.8276
4880	—	0.4655	—	—	—	0.8295
4900	—	0.4666	—	—	—	0.8314
4920	—	0.4677	—	—	—	0.8327
4940	—	0.4687	—	—	—	0.8340
4960	—	0.4698	—	—	—	0.8353
4980	—	0.4709	—	—	—	0.8366
5000	—	0.4719	—	—	—	0.8379
5020	—	0.4730	—	—	—	0.8388
5040	—	0.4741	—	—	—	0.8397
5060	—	0.4752	—	—	—	0.8406
5080	—	0.4762	—	—	—	0.8415

Table 4—Continued

$\lambda$	$u$	$g$	$r$	$i$	$z$	$T_{1.3airmass}$
5100	—	0.4770	—	—	—	0.8423
5120	—	0.4765	—	—	—	0.8432
5140	—	0.4753	—	—	—	0.8441
5160	—	0.4731	—	—	—	0.8450
5180	—	0.4704	—	—	—	0.8458
5200	—	0.4672	—	—	—	0.8467
5220	—	0.4625	—	—	—	0.8477
5240	—	0.4512	—	—	—	0.8487
5260	—	0.4326	—	—	—	0.8497
5280	—	0.3996	—	—	—	0.8507
5300	—	0.3429	—	—	—	0.8517
5320	—	0.2768	—	—	—	0.8527
5340	—	0.2013	—	—	—	0.8537
5360	—	0.1397	—	—	—	0.8547
5380	—	0.0899	0.0002	—	—	0.8557
5400	—	0.0585	0.0018	—	—	0.8567
5420	—	0.0398	0.0050	—	—	0.8571
5440	—	0.0269	0.0105	—	—	0.8576
5460	—	0.0189	0.0225	—	—	0.8580
5480	—	0.0136	0.0452	—	—	0.8585
5500	—	0.0096	0.0751	—	—	0.8589
5520	—	0.0068	0.1175	—	—	0.8594
5540	—	0.0051	0.1641	—	—	0.8598
5560	—	0.0037	0.2118	—	—	0.8602
5580	—	0.0024	0.2567	—	—	0.8607
5600	—	0.0013	0.2979	—	—	0.8611
5620	—	0.0002	0.3368	—	—	0.8616
5640	—	—	0.3724	—	—	0.8620
5660	—	—	0.4042	—	—	0.8625
5680	—	—	0.4327	—	—	0.8629
5700	—	—	0.4531	—	—	0.8634
5720	—	—	0.4667	—	—	0.8638
5740	—	—	0.4774	—	—	0.8643
5760	—	—	0.4868	—	—	0.8647
5780	—	—	0.4949	—	—	0.8652
5800	—	—	0.5019	—	—	0.8656
5820	—	—	0.5068	—	—	0.8672
5840	—	—	0.5118	—	—	0.8688
5860	—	—	0.5162	—	—	0.8704
5880	—	—	0.5187	—	—	0.8720
5900	—	—	0.5212	—	—	0.8736
5920	—	—	0.5237	—	—	0.8752
5940	—	—	0.5262	—	—	0.8768
5960	—	—	0.5287	—	—	0.8783
5980	—	—	0.5309	—	—	0.8799
6000	—	—	0.5323	—	—	0.8815
6020	—	—	0.5336	—	—	0.8841
6040	—	—	0.5349	—	—	0.8866
6060	—	—	0.5362	—	—	0.8891
6080	—	—	0.5370	—	—	0.8917
6100	—	—	0.5361	—	—	0.8942
6120	—	—	0.5352	—	—	0.8961
6140	—	—	0.5342	—	—	0.8980
6160	—	—	0.5333	—	—	0.8998

Table 4—Continued

$\lambda$	$u$	$g$	$r$	$i$	$z$	$T_{1.3airmass}$
6180	—	—	0.5333	—	—	0.9017
6200	—	—	0.5358	—	—	0.9036
6220	—	—	0.5383	—	—	0.9048
6240	—	—	0.5409	—	—	0.9059
6260	—	—	0.5434	—	—	0.9071
6280	—	—	0.5454	—	—	0.9083
6300	—	—	0.5462	—	—	0.9095
6320	—	—	0.5470	—	—	0.9104
6340	—	—	0.5477	—	—	0.9114
6360	—	—	0.5485	—	—	0.9123
6380	—	—	0.5488	—	—	0.9133
6400	—	—	0.5480	—	—	0.9142
6420	—	—	0.5472	—	—	0.9152
6440	—	—	0.5464	—	—	0.9161
6460	—	—	0.5455	—	—	0.9171
6480	—	—	0.5449	—	—	0.9180
6500	—	—	0.5450	—	—	0.9190
6520	—	—	0.5450	—	—	0.9194
6540	—	—	0.5447	—	—	0.9198
6560	—	—	0.5435	—	—	0.9202
6580	—	—	0.5423	—	—	0.9206
6600	—	—	0.5394	0.0002	—	0.9210
6620	—	—	0.5324	0.0008	—	0.9214
6640	—	—	0.5190	0.0012	—	0.9217
6660	—	—	0.4992	0.0017	—	0.9221
6680	—	—	0.4683	0.0026	—	0.9225
6700	—	—	0.4230	0.0046	—	0.9228
6720	—	—	0.3685	0.0080	—	0.9232
6740	—	—	0.3030	0.0131	—	0.9236
6760	—	—	0.2344	0.0226	—	0.9239
6780	—	—	0.1724	0.0365	—	0.9243
6800	—	—	0.1212	0.0560	—	0.9246
6820	—	—	0.0842	0.0834	—	0.9250
6840	—	—	0.0556	0.1162	—	0.9027
6860	—	—	0.0370	0.1553	—	0.8804
6880	—	—	0.0273	0.1952	—	0.8581
6900	—	—	0.0201	0.2377	—	0.8722
6920	—	—	0.0130	0.2839	—	0.8863
6940	—	—	0.0097	0.3222	—	0.9004
6960	—	—	0.0076	0.3565	—	0.9145
6980	—	—	0.0054	0.3869	—	0.9286
7000	—	—	0.0036	0.4104	—	0.9298
7020	—	—	0.0019	0.4301	—	0.9301
7040	—	—	0.0003	0.4458	—	0.9305
7060	—	—	—	0.4565	—	0.9308
7080	—	—	—	0.4648	—	0.9312
7100	—	—	—	0.4706	—	0.9315
7120	—	—	—	0.4764	—	0.9319
7140	—	—	—	0.4791	—	0.9322
7160	—	—	—	0.4814	—	0.8928
7180	—	—	—	0.4823	—	0.8533
7200	—	—	—	0.4815	—	0.8703
7220	—	—	—	0.4806	—	0.8873
7240	—	—	—	0.4771	—	0.8896

Table 4—Continued

$\lambda$	$u$	$g$	$r$	$i$	$z$	$T_{1.3airmass}$
7260	—	—	—	0.4732	—	0.8919
7280	—	—	—	0.4694	—	0.8942
7300	—	—	—	0.4655	—	0.8966
7320	—	—	—	0.4617	—	0.9156
7340	—	—	—	0.4578	—	0.9346
7360	—	—	—	0.4539	—	0.9358
7380	—	—	—	0.4505	—	0.9365
7400	—	—	—	0.4477	—	0.9371
7420	—	—	—	0.4449	—	0.9371
7440	—	—	—	0.4421	—	0.9371
7460	—	—	—	0.4393	—	0.9371
7480	—	—	—	0.4364	—	0.9371
7500	—	—	—	0.4335	—	0.9371
7520	—	—	—	0.4306	—	0.9371
7540	—	—	—	0.4264	—	0.9371
7560	—	—	—	0.4220	—	0.9371
7580	—	—	—	0.4176	—	0.9209
7600	—	—	—	0.4132	—	0.5647
7620	0.000003	—	—	0.4088	—	0.6334
7640	0.000044	—	—	0.4042	—	0.6037
7660	0.000149	—	—	0.3996	—	0.7830
7680	0.000258	—	—	0.3951	0.0000	0.9396
7700	0.000397	—	—	0.3905	0.0000	0.9407
7720	0.000553	—	—	0.3860	0.0001	0.9410
7740	0.000676	—	—	0.3815	0.0001	0.9412
7760	0.000675	—	—	0.3770	0.0001	0.9415
7780	0.000551	—	—	0.3725	0.0001	0.9417
7800	0.000403	—	—	0.3680	0.0002	0.9420
7820	0.000276	—	—	0.3636	0.0002	0.9422
7840	0.000179	—	—	0.3610	0.0002	0.9424
7860	0.000093	—	—	0.3586	0.0003	0.9427
7880	0.000044	—	—	0.3562	0.0004	0.9429
7900	0.000026	—	—	0.3539	0.0006	0.9432
7920	0.000011	—	—	0.3515	0.0008	0.9433
7940	0.000007	—	—	0.3492	0.0010	0.9434
7960	—	—	—	0.3469	0.0012	0.9435
7980	—	—	—	0.3449	0.0016	0.9437
8000	—	—	—	0.3432	0.0023	0.9438
8020	—	—	—	0.3411	0.0030	0.9439
8040	—	—	—	0.3388	0.0044	0.9440
8060	—	—	—	0.3362	0.0059	0.9442
8080	—	—	—	0.3328	0.0078	0.9443
8100	—	—	—	0.3279	0.0105	0.9444
8120	—	—	—	0.3215	0.0132	0.9205
8140	—	—	—	0.3043	0.0171	0.8966
8160	—	—	—	0.2763	0.0212	0.8966
8180	—	—	—	0.2379	0.0257	0.8966
8200	—	—	—	0.1857	0.0309	0.8966
8220	—	—	—	0.1355	0.0362	0.8966
8240	—	—	—	0.0874	0.0415	0.8966
8260	—	—	—	0.0578	0.0467	0.8966
8280	—	—	—	0.0360	0.0519	0.8966
8300	—	—	—	0.0212	0.0570	0.8966
8320	—	—	—	0.0144	0.0621	0.9167

Table 4—Continued

$\lambda$	$u$	$g$	$r$	$i$	$z$	$T_{1.3airmass}$
8340	—	—	—	0.0094	0.0664	0.9368
8360	—	—	—	0.0061	0.0705	0.9469
8380	—	—	—	0.0020	0.0742	0.9470
8400	—	—	—	—	0.0773	0.9470
8420	—	—	—	—	0.0803	0.9471
8440	—	—	—	—	0.0824	0.9472
8460	—	—	—	—	0.0845	0.9473
8480	—	—	—	—	0.0861	0.9474
8500	—	—	—	—	0.0871	0.9475
8520	—	—	—	—	0.0882	0.9476
8540	—	—	—	—	0.0893	0.9477
8560	—	—	—	—	0.0904	0.9478
8580	—	—	—	—	0.0911	0.9479
8600	—	—	—	—	0.0912	0.9480
8620	—	—	—	—	0.0913	0.9481
8640	—	—	—	—	0.0915	0.9482
8660	—	—	—	—	0.0917	0.9483
8680	—	—	—	—	0.0914	0.9484
8700	—	—	—	—	0.0906	0.9484
8720	—	—	—	—	0.0898	0.9485
8740	—	—	—	—	0.0889	0.9486
8760	—	—	—	—	0.0881	0.9487
8780	—	—	—	—	0.0869	0.9488
8800	—	—	—	—	0.0854	0.9489
8820	—	—	—	—	0.0838	0.9490
8840	—	—	—	—	0.0822	0.9491
8860	—	—	—	—	0.0806	0.9492
8880	—	—	—	—	0.0790	0.9493
8900	—	—	—	—	0.0772	0.9493
8920	—	—	—	—	0.0755	0.9190
8940	—	—	—	—	0.0738	0.8888
8960	—	—	—	—	0.0720	0.8585
8980	—	—	—	—	0.0704	0.8282
9000	—	—	—	—	0.0688	0.8387
9020	—	—	—	—	0.0672	0.8492
9040	—	—	—	—	0.0656	0.8597
9060	—	—	—	—	0.0640	0.8701
9080	—	—	—	—	0.0625	0.8701
9100	—	—	—	—	0.0612	0.8701
9120	—	—	—	—	0.0598	0.8701
9140	—	—	—	—	0.0585	0.8701
9160	—	—	—	—	0.0571	0.8701
9180	—	—	—	—	0.0559	0.8701
9200	—	—	—	—	0.0547	0.8701
9220	—	—	—	—	0.0535	0.8701
9240	—	—	—	—	0.0523	0.8701
9260	—	—	—	—	0.0511	0.8701
9280	—	—	—	—	0.0499	0.8043
9300	—	—	—	—	0.0487	0.7385
9320	—	—	—	—	0.0475	0.6727
9340	—	—	—	—	0.0463	0.6069
9360	—	—	—	—	0.0451	0.5861
9380	—	—	—	—	0.0440	0.6104
9400	—	—	—	—	0.0430	0.6346

Table 4—Continued

$\lambda$	$u$	$g$	$r$	$i$	$z$	$T_{1.3airmass}$
9420	—	—	—	—	0.0420	0.6588
9440	—	—	—	—	0.0410	0.6365
9460	—	—	—	—	0.0400	0.6142
9480	—	—	—	—	0.0390	0.6331
9500	—	—	—	—	0.0379	0.6520
9520	—	—	—	—	0.0369	0.6491
9540	—	—	—	—	0.0358	0.6461
9560	—	—	—	—	0.0347	0.6728
9580	—	—	—	—	0.0337	0.6994
9600	—	—	—	—	0.0327	0.7322
9620	—	—	—	—	0.0317	0.7651
9640	—	—	—	—	0.0307	0.8003
9660	—	—	—	—	0.0297	0.8355
9680	—	—	—	—	0.0287	0.8707
9700	—	—	—	—	0.0276	0.9059
9720	—	—	—	—	0.0266	0.8880
9740	—	—	—	—	0.0256	0.8701
9760	—	—	—	—	0.0245	0.8846
9780	—	—	—	—	0.0235	0.8990
9800	—	—	—	—	0.0226	0.9135
9820	—	—	—	—	0.0216	0.9279
9840	—	—	—	—	0.0206	0.9423
9860	—	—	—	—	0.0196	0.9568
9880	—	—	—	—	0.0186	0.9568
9900	—	—	—	—	0.0176	0.9568
9920	—	—	—	—	0.0166	0.9568
9940	—	—	—	—	0.0156	0.9568
9960	—	—	—	—	0.0147	0.9568
9980	—	—	—	—	0.0138	0.9569
10000	—	—	—	—	0.0132	0.9569
10020	—	—	—	—	0.0125	0.9569
10040	—	—	—	—	0.0119	0.9569
10060	—	—	—	—	0.0113	0.9569
10080	—	—	—	—	0.0106	0.9570
10100	—	—	—	—	0.0099	0.9570
10120	—	—	—	—	0.0093	0.9570
10140	—	—	—	—	0.0086	0.9570
10160	—	—	—	—	0.0080	0.9570
10180	—	—	—	—	0.0074	0.9571
10200	—	—	—	—	0.0070	0.9571
10220	—	—	—	—	0.0065	0.9571
10240	—	—	—	—	0.0061	0.9571
10260	—	—	—	—	0.0056	0.9571
10280	—	—	—	—	0.0052	0.9571
10300	—	—	—	—	0.0047	0.9572
10320	—	—	—	—	0.0042	0.9572
10340	—	—	—	—	0.0038	0.9572
10360	—	—	—	—	0.0033	0.9572
10380	—	—	—	—	0.0030	0.9572
10400	—	—	—	—	0.0029	0.9573
10420	—	—	—	—	0.0027	0.9573
10440	—	—	—	—	0.0026	0.9573
10460	—	—	—	—	0.0024	0.9573
10480	—	—	—	—	0.0022	0.9573

Table 4—Continued

$\lambda$	$u$	$g$	$r$	$i$	$z$	$T_{1.3airmass}$
10500	—	—	—	—	0.0021	0.9574
10520	—	—	—	—	0.0019	0.9574
10540	—	—	—	—	0.0018	0.9574
10560	—	—	—	—	0.0016	0.9574
10580	—	—	—	—	0.0015	0.9574
10600	—	—	—	—	0.0014	0.9574
10620	—	—	—	—	0.0013	0.9575
10640	—	—	—	—	0.0012	0.9575
10660	—	—	—	—	0.0012	0.9575
10680	—	—	—	—	0.0011	0.9575
10700	—	—	—	—	0.0010	0.9575
10720	—	—	—	—	0.0009	0.9576
10740	—	—	—	—	0.0008	0.9576
10760	—	—	—	—	0.0007	0.9576
10780	—	—	—	—	0.0007	0.9576
10800	—	—	—	—	0.0007	0.9576
10820	—	—	—	—	0.0006	0.9577
10840	—	—	—	—	0.0006	0.9577
10860	—	—	—	—	0.0006	0.9577
10880	—	—	—	—	0.0005	0.9577
10900	—	—	—	—	0.0005	0.9577
10920	—	—	—	—	0.0005	0.9577
10940	—	—	—	—	0.0004	0.9578
10960	—	—	—	—	0.0004	0.9578
10980	—	—	—	—	0.0004	0.9578
11000	—	—	—	—	0.0003	0.9578
11020	—	—	—	—	0.0003	0.9578
11040	—	—	—	—	0.0002	0.9579
11060	—	—	—	—	0.0002	0.9579
11080	—	—	—	—	0.0002	0.9579
11100	—	—	—	—	0.0001	0.9579
11120	—	—	—	—	0.0001	0.9579
11140	—	—	—	—	0.0001	0.9580
11160	—	—	—	—	0.0000	0.9580

Table 5: Summary of the uncertainties in the effective wavelength

source	uncertainty ( $\text{\AA}$ )	band	comments
monochromator repeatability	$\pm 3$	all	r.m.s.
incident angle	-2 – -3	g, r, i	half of red cutoff shifts
filter temperature	7, 15, 21, 51	g, r, i, z	peak-to-peak, color glass temperature effect
aging	$\approx -30$	u	CCD coating?
CCD sensitivity?	$\approx \pm 30$	z	temperature effect?

Table 6: Brightness of BD+17°4708 in AB<sub>95</sub> without atmospheric extinction

	$u$	$g$	$r$	$i$	$z$
F96 standard	10.559	9.636	9.353	9.251	9.230
USNO 1m	10.558	9.644	9.353	9.252	9.230
PT-new	10.565	9.640	9.356	9.252	9.230
2.5m reference	10.525	9.670	9.361	9.257	9.228
SDSS public web site (2001)	10.560	9.671	9.361	9.257	9.229

Table 7: Characteristics of the response functions and brightness of BD+17°4708 with atmospheric transmission at 1.3 airmass. Atmospheric extinction in flux itself is removed in brightness.

	<i>u</i>	<i>g</i>	<i>r</i>	<i>i</i>	<i>z</i>
F96 standard $\lambda_{\text{eff}}$	3537	4753	6209	7619	9032
USNO 1m $\lambda_{\text{eff}}$	3539	4731	6210	7609	9030
PT-new $\lambda_{\text{eff}}$	3534	4742	6189	7595	9032
2.5m reference $\lambda_{\text{eff}}$	3568	4653	6148	7468	8863
BD+17°4708 with F96 standard (1.3 airmass)	10.520	9.628	9.353	9.251	9.231
BD+17°4708 with USNO 1m (1.3 airmass)	10.519	9.635	9.353	9.252	9.231
BD+17°4708 with PT-new (1.3 airmass)	10.527	9.632	9.355	9.252	9.231
BD+17°4708 with 2.5m reference (1.3 airmass)	10.489	9.662	9.360	9.257	9.228
BD+17°4708 with SDSS “public” web (1.3 airmass)	10.518	9.662	9.360	9.257	9.229



Fig. 1.— Monochromatic illumination system overview. (1) lamp; (2) light condensation mirror system; (3) input slit; (4) monochromator; (5) shutter; (6) mirror switch to change the output direction; (7) integration sphere; (8) photodiode.

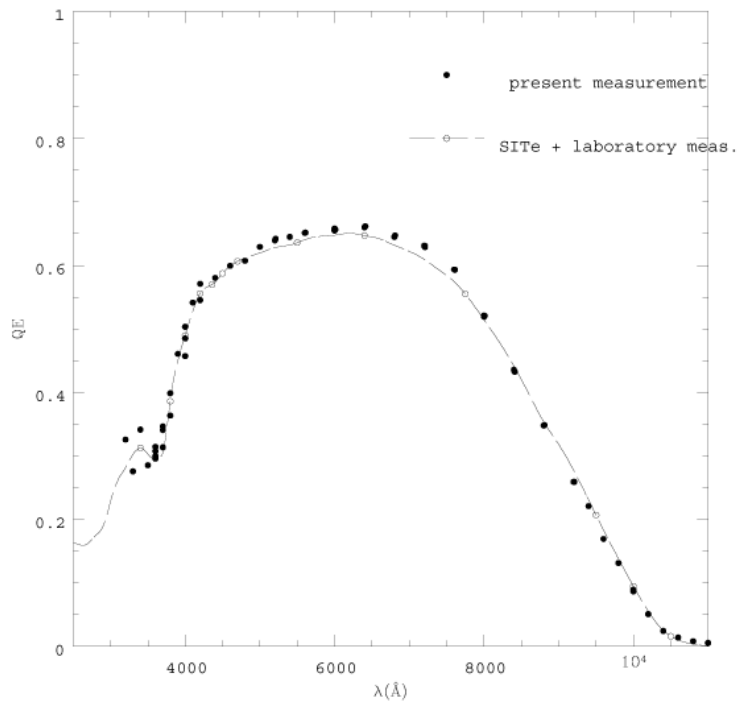


Fig. 2.— Response function (quantum efficiency) of the ultraviolet-enhancing coated thinned back-illuminated CCD used at the Photometric Telescope. The solid points are the measurement with the present system, and the dashed curve is the quantum efficiency for the same CCD measured at SITE at a room temperature, but tilted using a laboratory measurement (open points) at a cooled, operating temperature, used in F96.

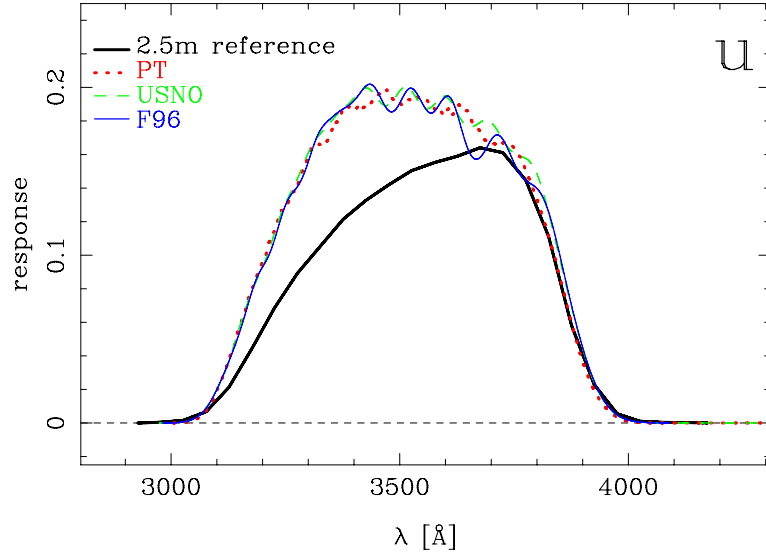


Fig. 3.— Response functions for the *u* band. The thick solid curve is the reference response function for the 2.5 m telescope imager defined in the text, thin solid curve is the F96 standard, the dashed curve is for the USNO 1m telescope system, and the dotted curve is for the SDSS Photometric Telescope (after the replacement of filters: see text)

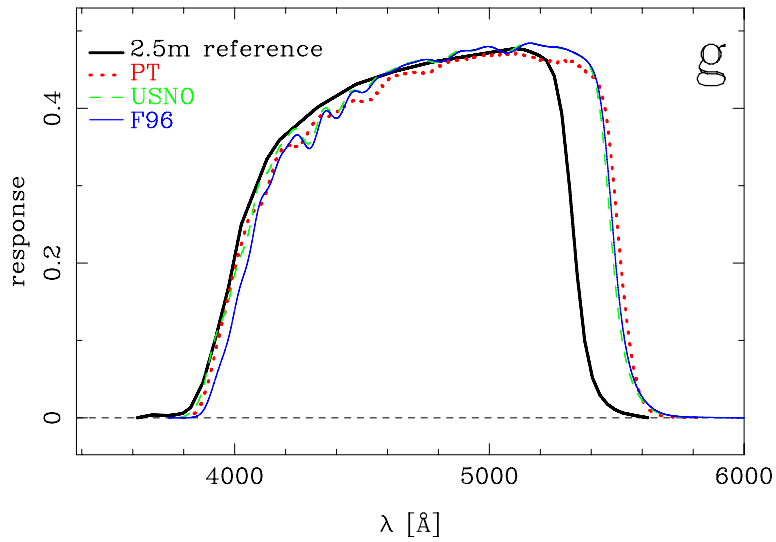


Fig. 4.— Same as Figure 2, but for the *g* band.

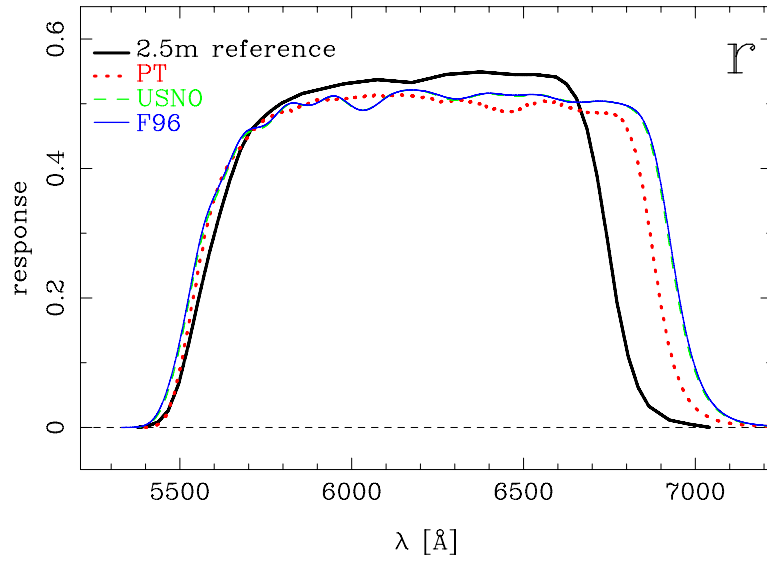


Fig. 5.— Same as Figure 2, but for the *r* band.

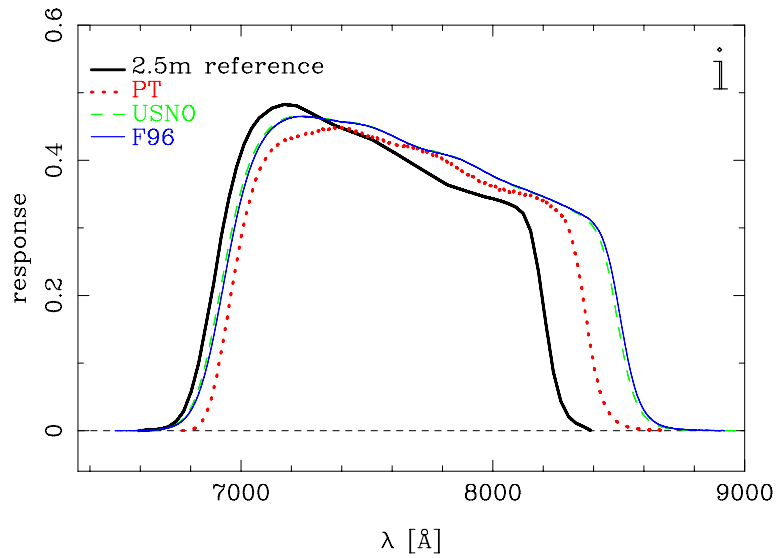


Fig. 6.— Same as Figure 2, but for the *i* band.

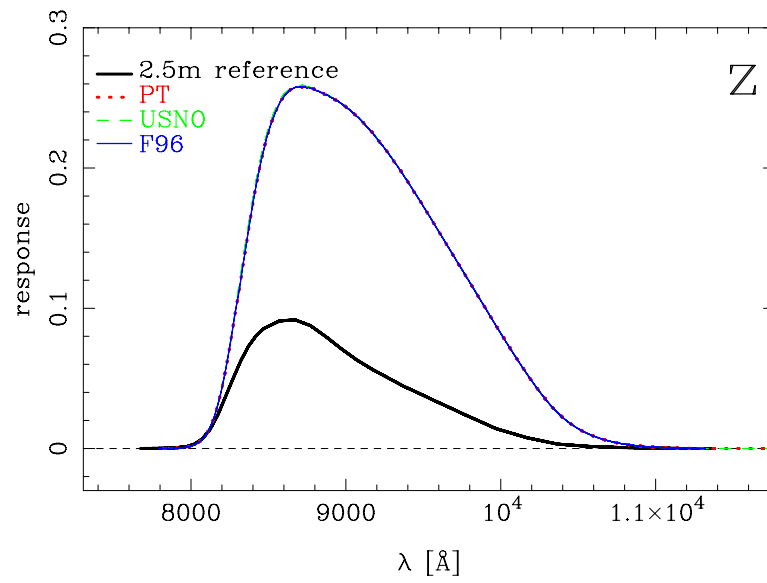


Fig. 7.— Same as Figure 2, but for the  $z$  band.

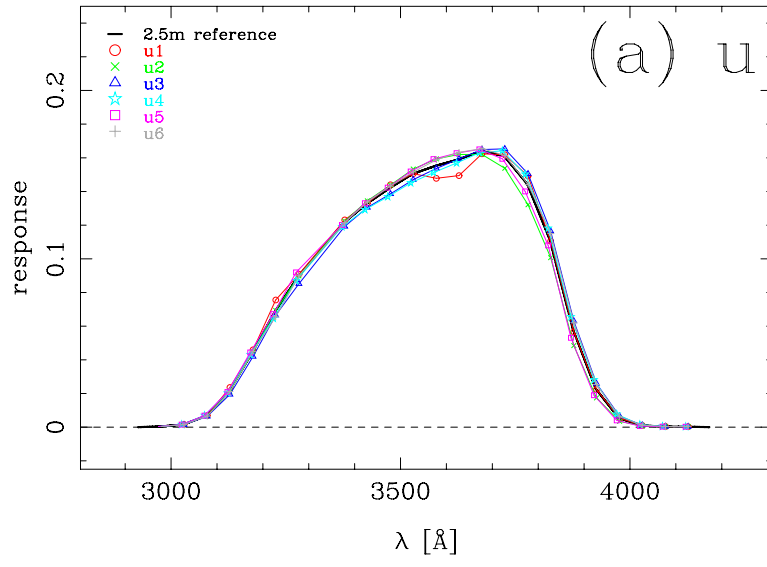


Fig. 8 (a).— Response function for each column of the detector in the main camera. (a) *u* band, (b) *g* band, (c) *r* band, (d) *i* band, (e) *z* band.

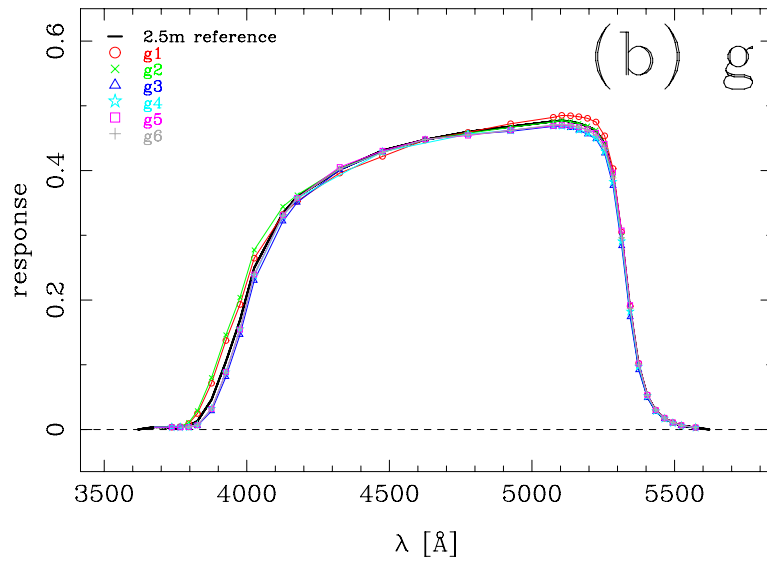


Fig. 8 (b).—

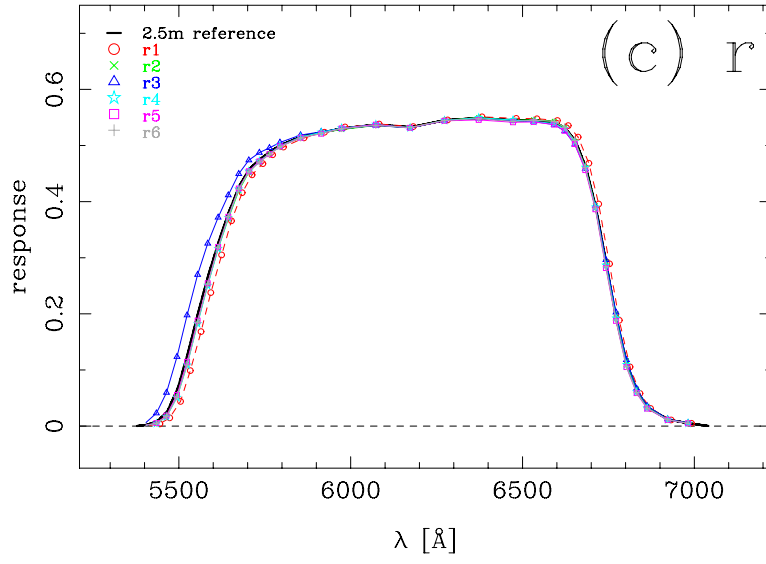


Fig. 8 (c).—

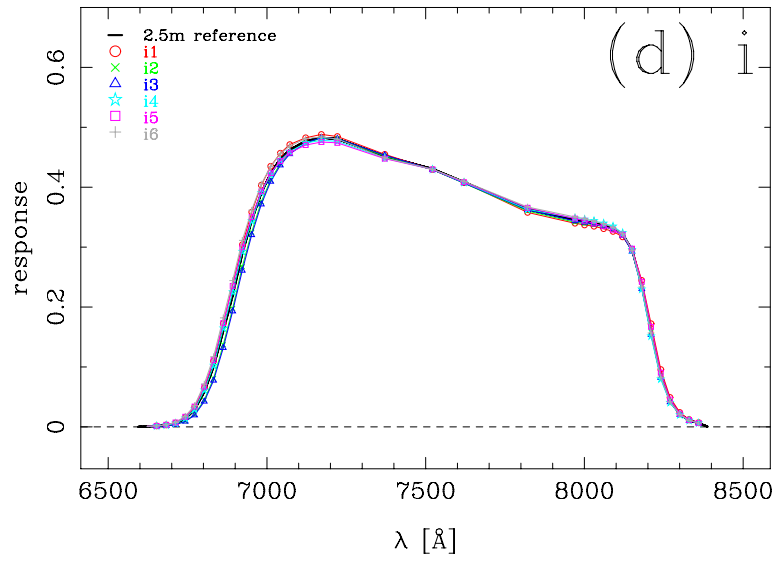


Fig. 8 (d).—

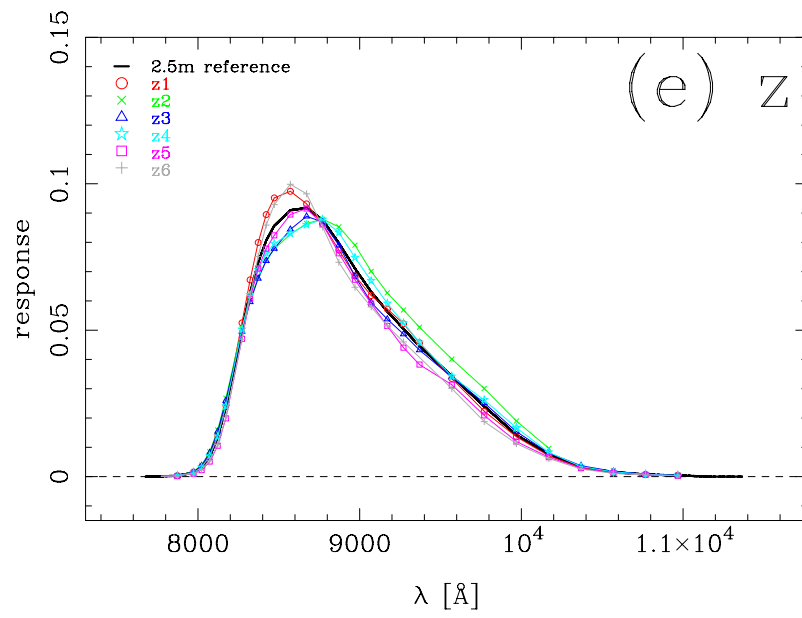


Fig. 8 (e).—

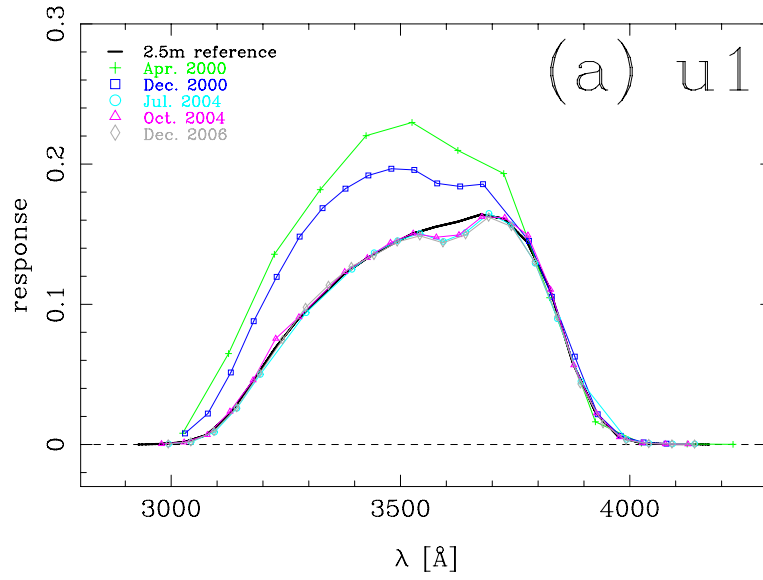


Fig. 9 (a).— Response functions at various epochs of measurements for the imager in the main camera. (a) *u* band, Camcol 1, (b) *g* band, Camcol 1, (c) *r* band Camcol 1, (d) *i* band, Camcol 1, (e) *z* band Camcol 1, and (f) red leak for the *u* band, Camcol 1.

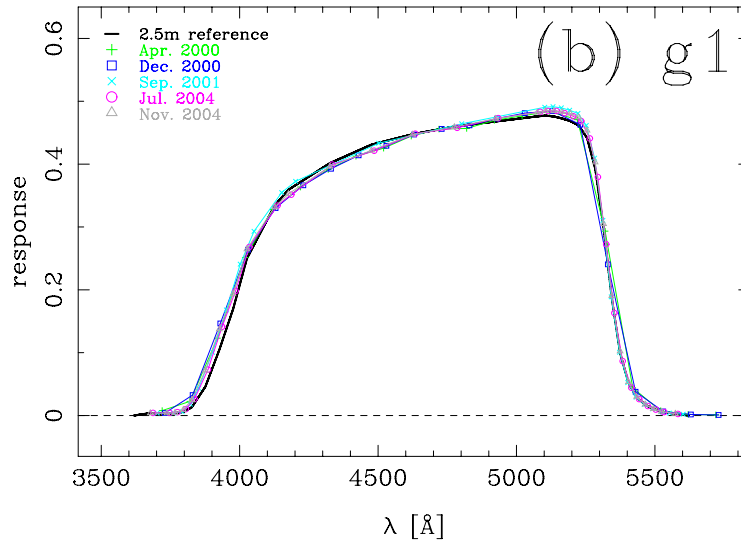


Fig. 9 (b).—

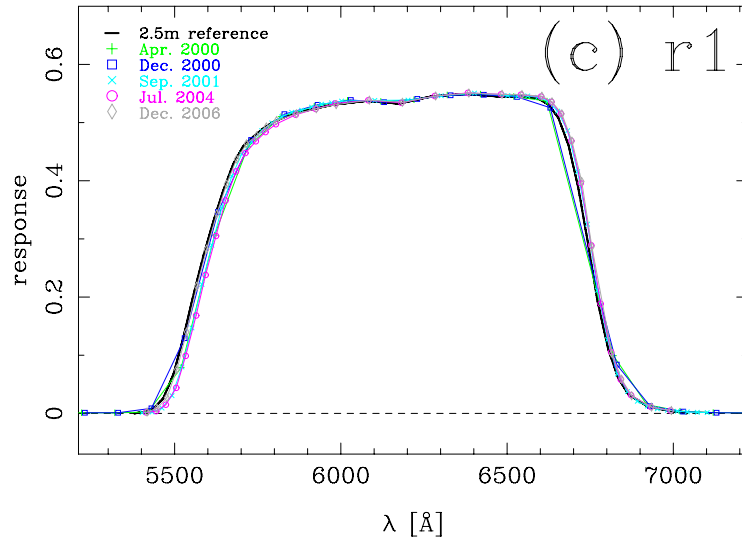


Fig. 9 (c).—

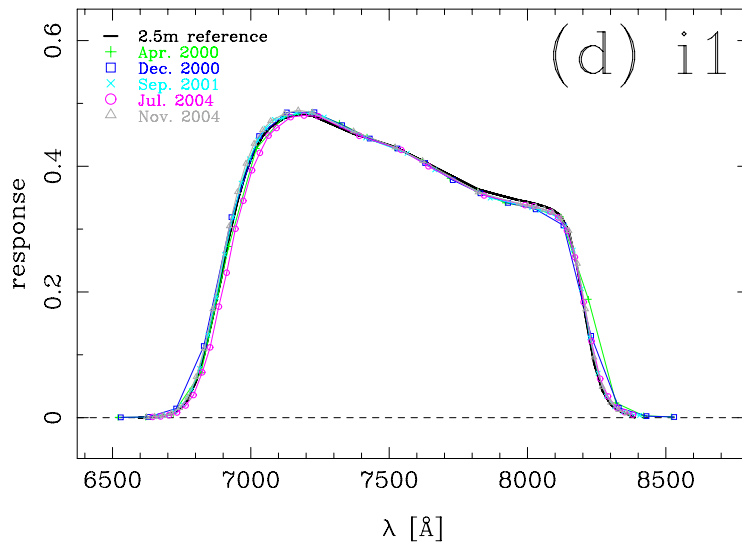


Fig. 9 (d).—

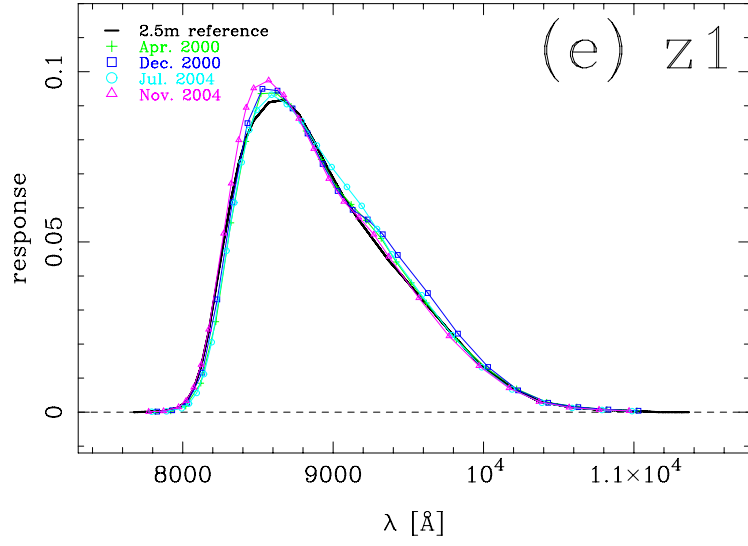


Fig. 9 (e).—

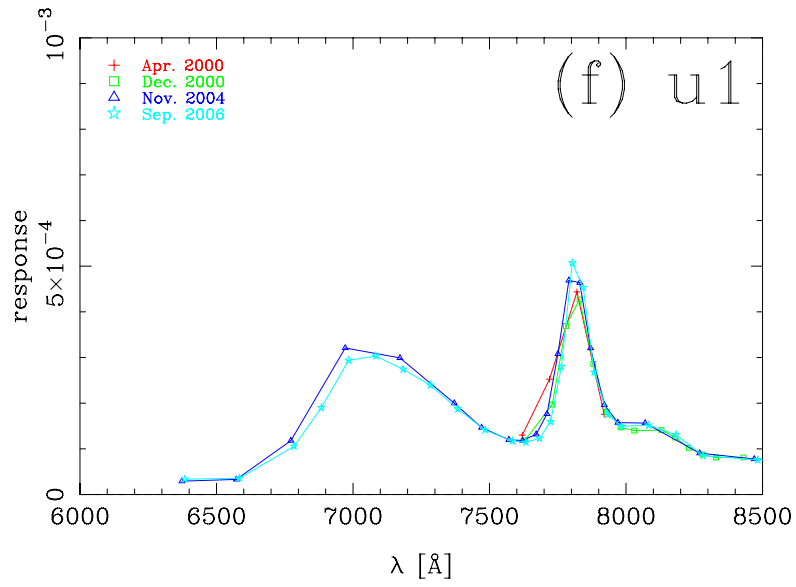


Fig. 9 (f).—

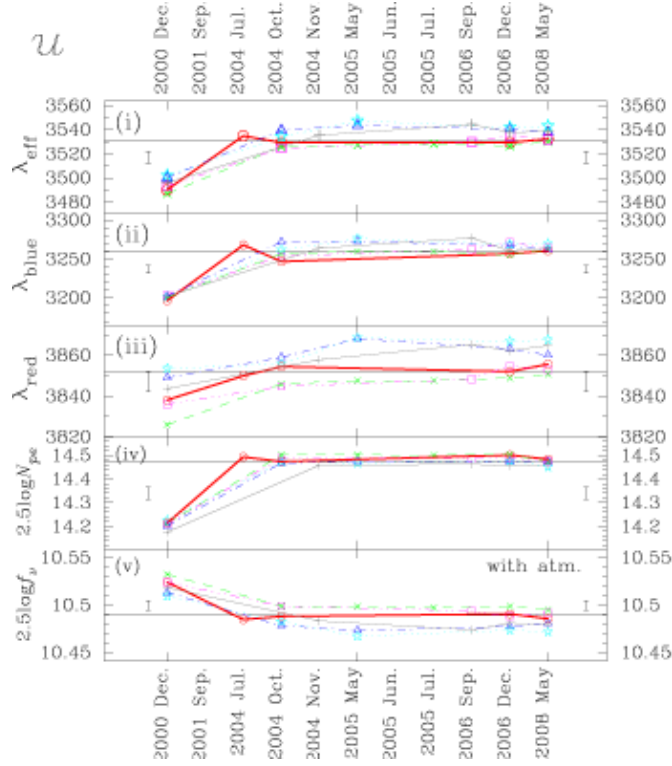


Fig. 10 (a).— Time variations of the response functions and their effects on photometry. From the top to the bottom: (i) the effective wavelength,  $\lambda_{\text{eff}}$ , (ii) 50%-response wavelengths of the blue edges, (iii) 50%-response wavelengths of the red edges, (iv) the detector sensitivity i.e, the quantity proportional to  $-2.5 \log N_{p.e.}$  (arbitrary unit) where  $N_{p.e.}$  is the number of photoelectrons in the detector, or brightness defined by eq. (3) but with the denominator set equal to unity. The star is BD+17°4708; (v) brightness of BD+17°4708 from eq. (3). The response function includes the effect of atmosphere at 1.3 airmass. The symbols are the same as in Fig. 8 (circle, cross, triangle, star, square, and plus present column 1-6, respectively). The horizontal line in each panel is for the reference response. In the panels (i), (ii), and (iii), the error bars show  $10\text{\AA}$ , and in (iv) and (v), they show 0.05 mag and 0.01 mag, respectively.

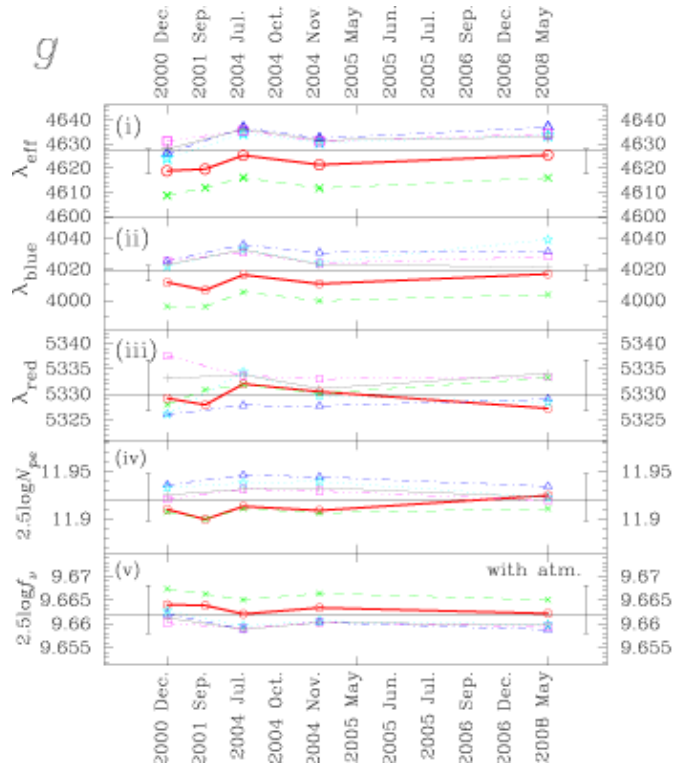


Fig. 10 (b).—

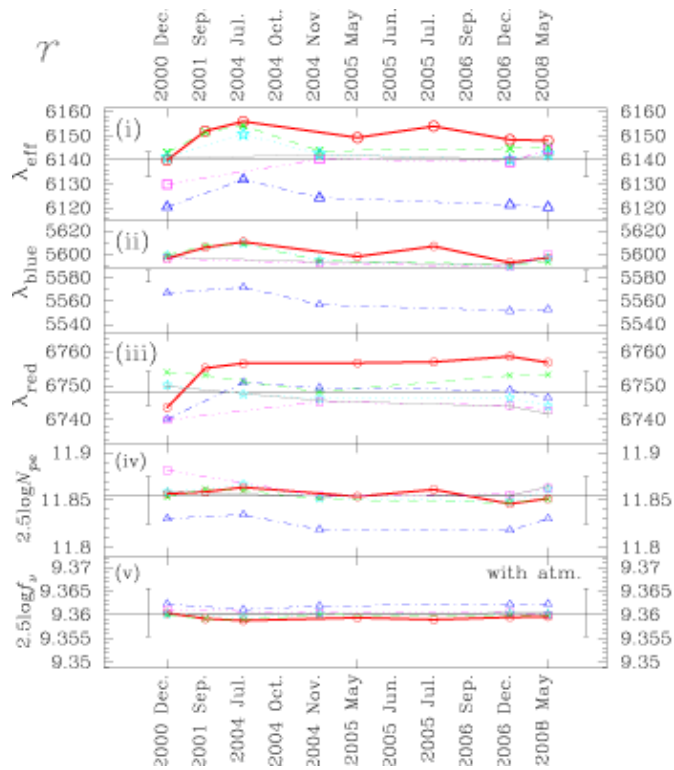


Fig. 10 (c).—

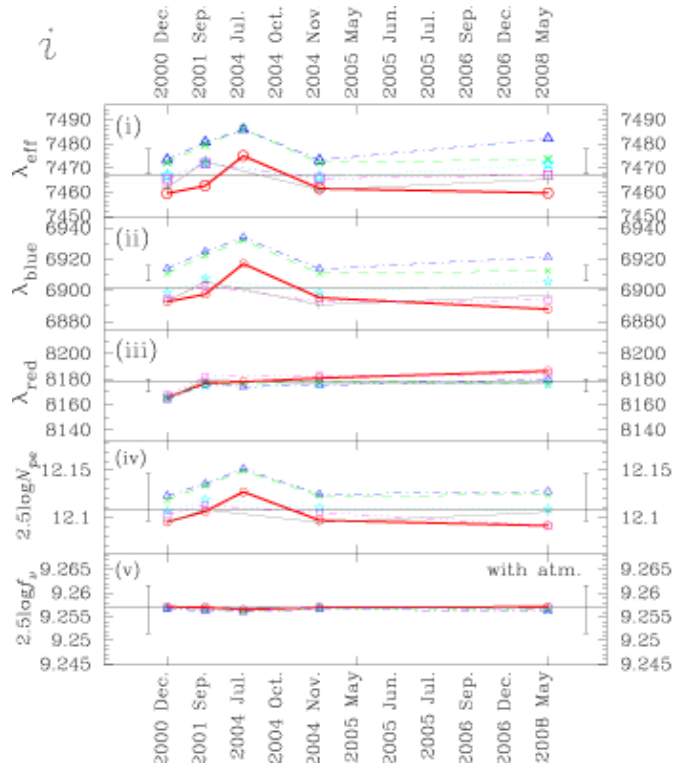


Fig. 10 (d).—

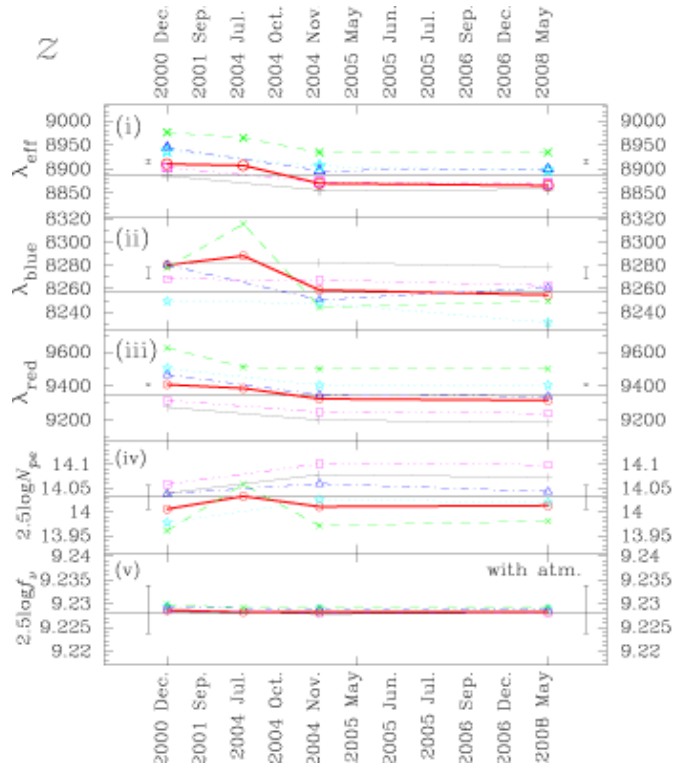


Fig. 10 (e).—

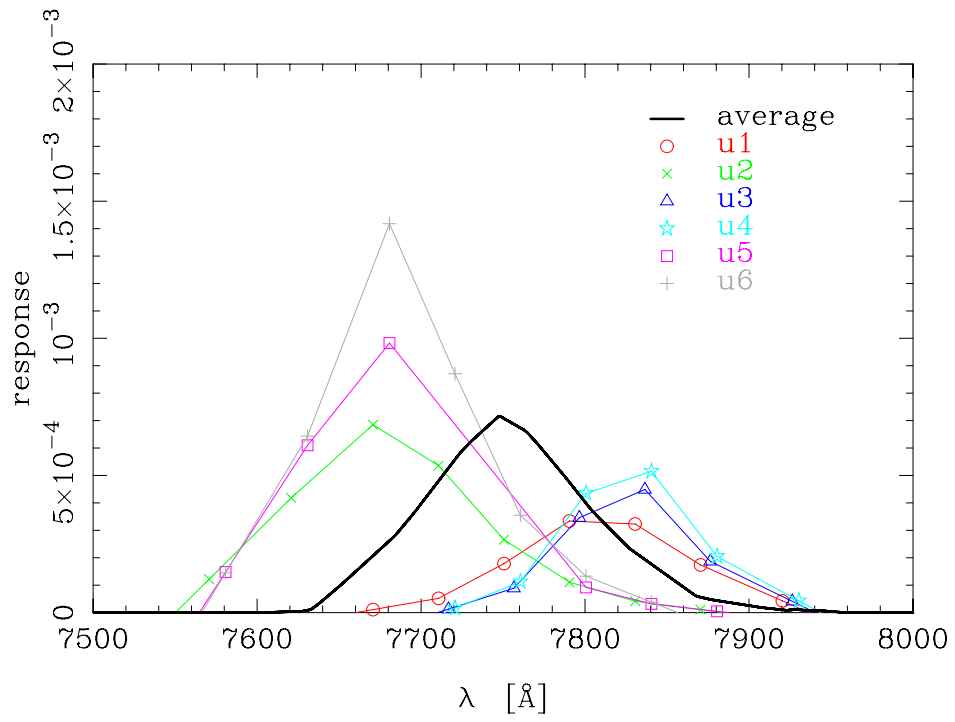


Fig. 11.— The u-band redleak response after subtraction of the possible scattered light. The thick line shows the average of all six columns.

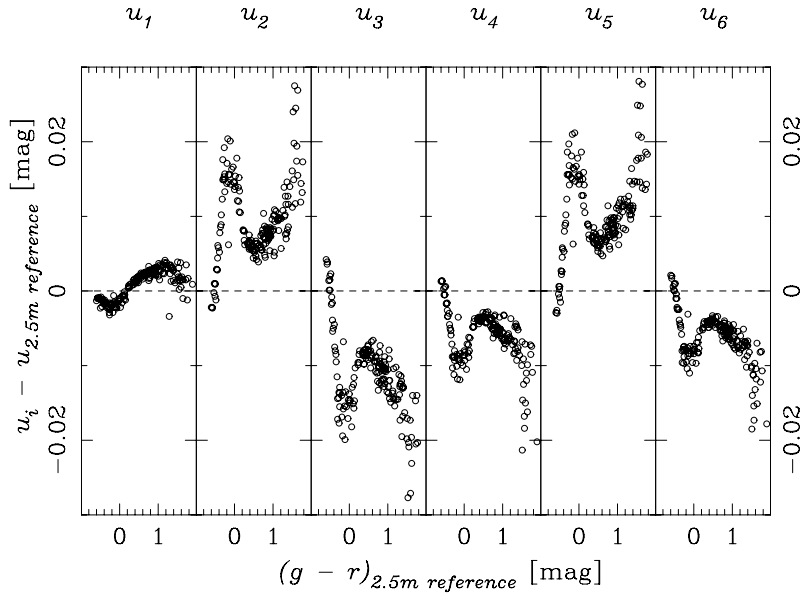


Fig. 12 (a).— Column to column colour variations expected in the  $u$  band as a function of  $g - r$  colour of stars. The response function involves atmospheric extinction at 1.3 airmass.

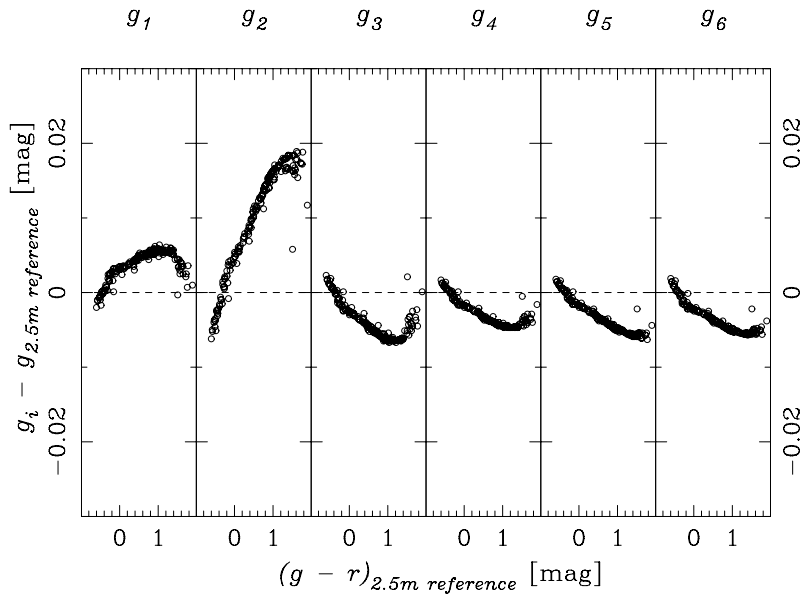


Fig. 12 (b).— The same as Fig.11(a) but in the  $g$  band.

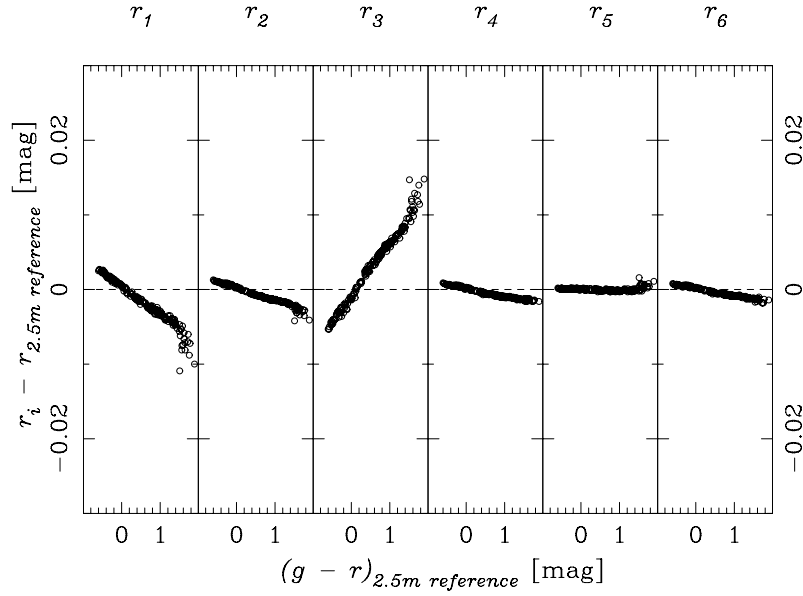


Fig. 12 (c).— The same as Fig.11(a) but in the  $r$  band.

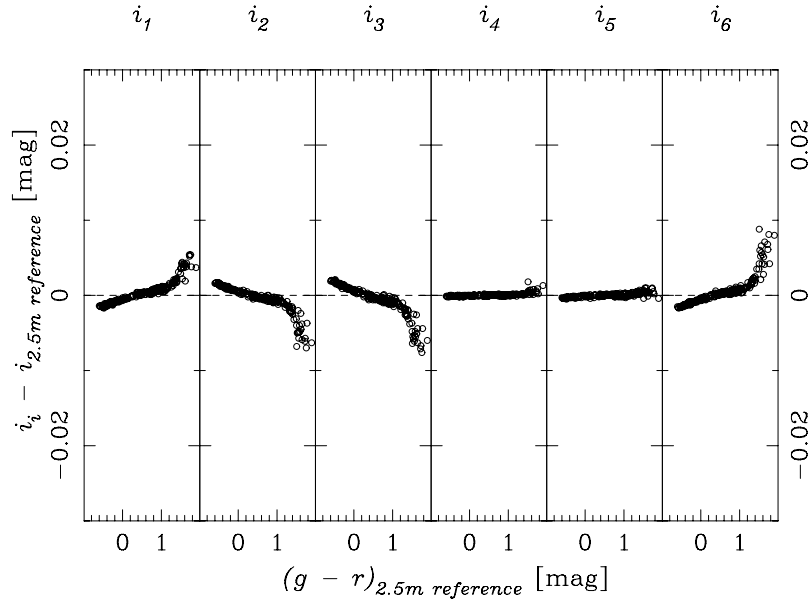


Fig. 12 (d).— The same as Fig.11(a) but in the  $i$  band.

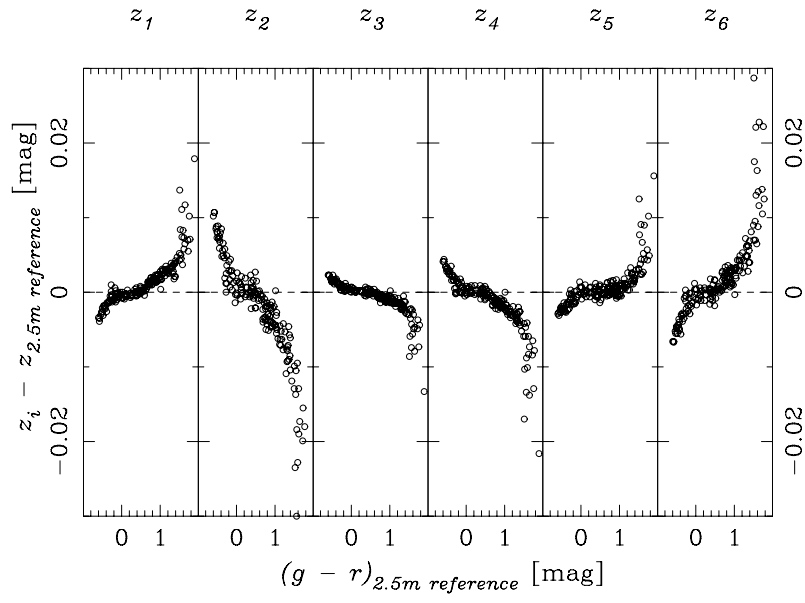


Fig. 12 (e).— The same as Fig.11(a) but in the  $z$  band.

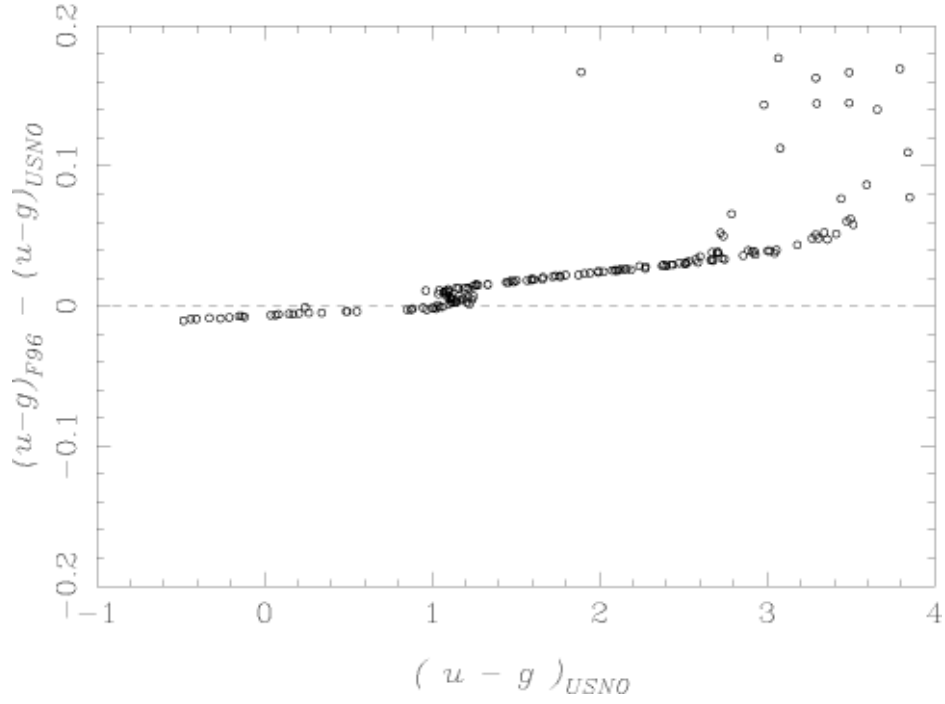


Fig. 13 (a).— Expected offset of  $u-g$  colour between the USNO photometric system and the original F96 standard,  $\Delta(u-g)_{AB} = (u-g)_{USNO} - (u-g)_{F96standard}$  plotted as a function of  $u-g$ . The response function involves atmospheric extinction.

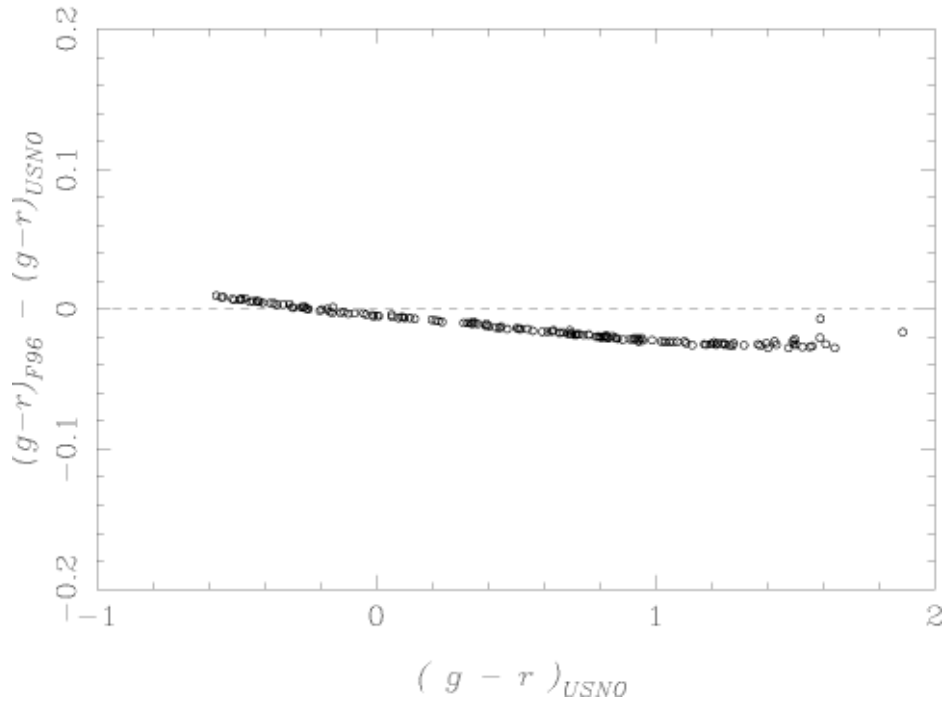


Fig. 13 (b).— The same as Fig.12(a) but for  $g-r$ .

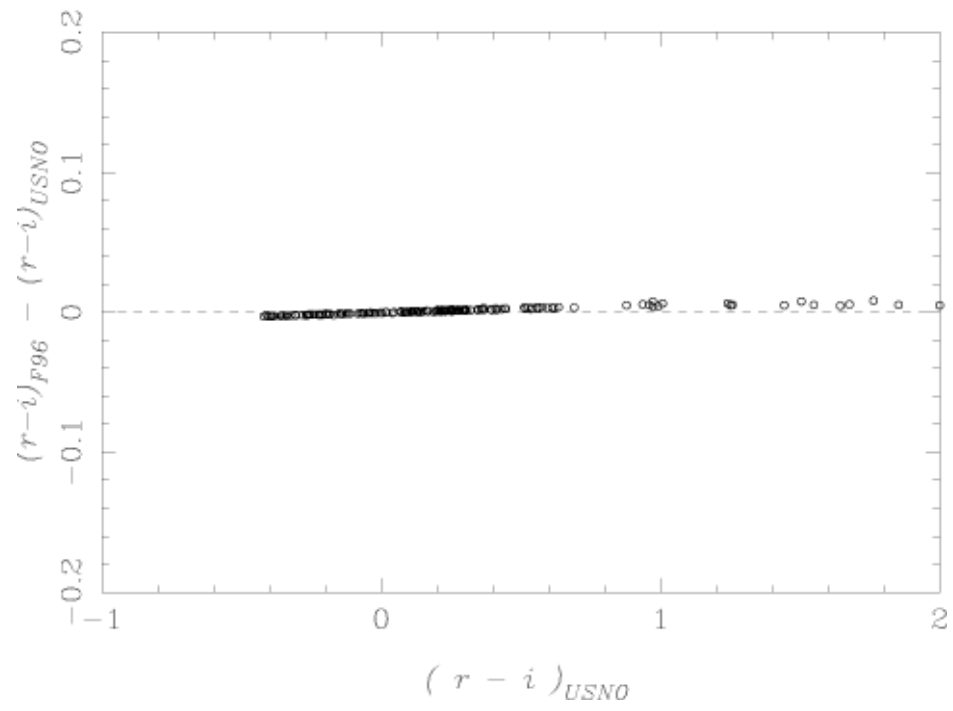


Fig. 13 (c).— The same as Fig.12(a) but for  $r - i$ .

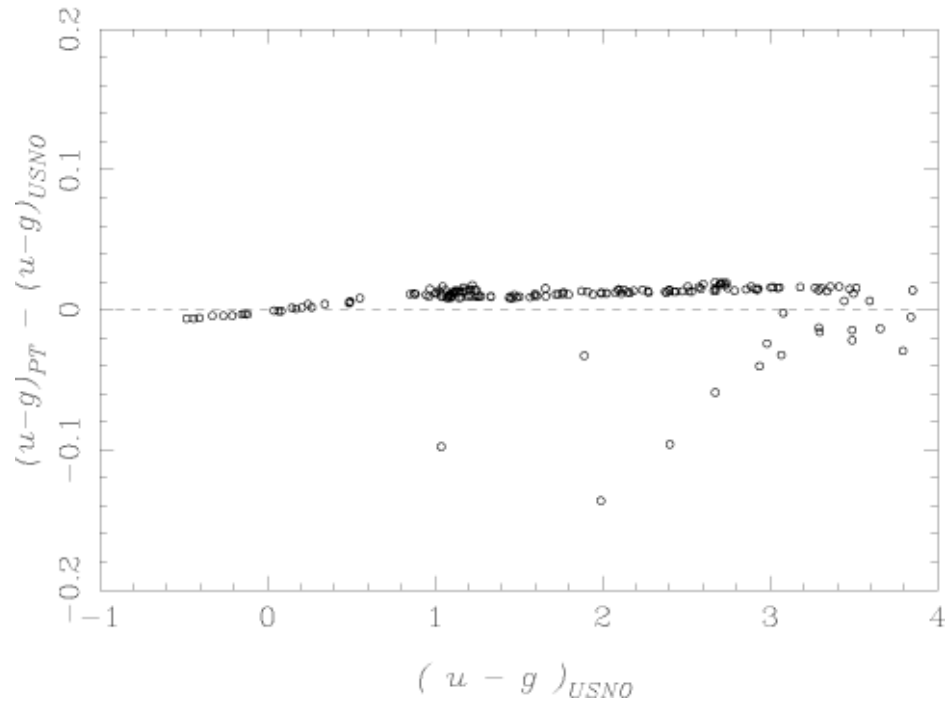


Fig. 14 (a).— Expected offset of  $u-g$  colour between the Photometric Telescope PT-new and the USNO photometric system,  $\Delta(u-g)_{AB} = (u-g)_{PT\text{-new}} - (u-g)_{USNO}$  plotted as a function of  $u-g$ .

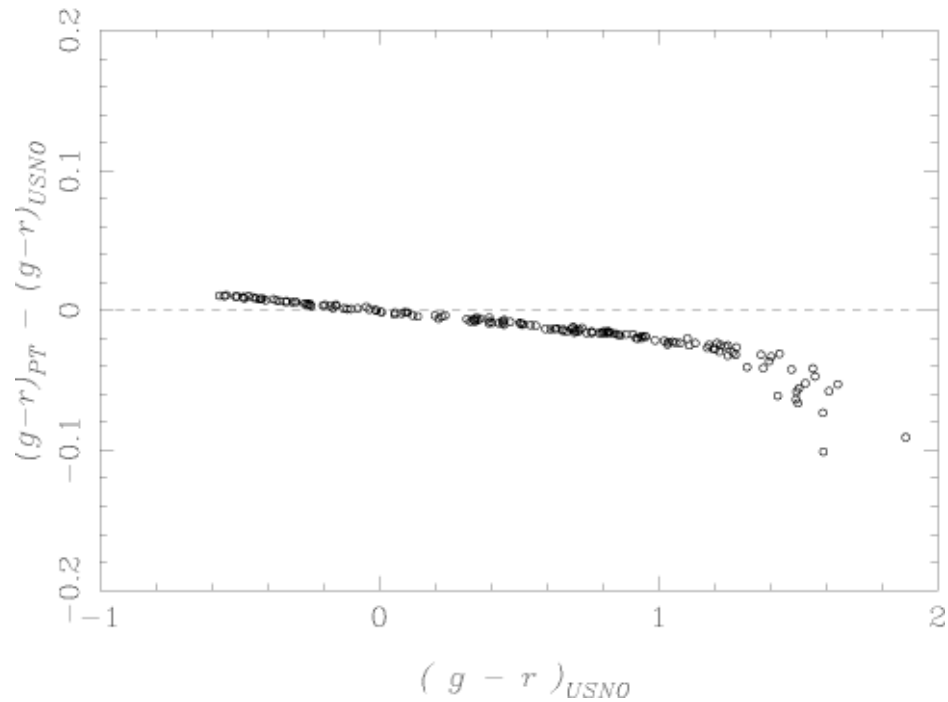


Fig. 14 (b).— The same as Fig.13(a) but for  $g-r$ .

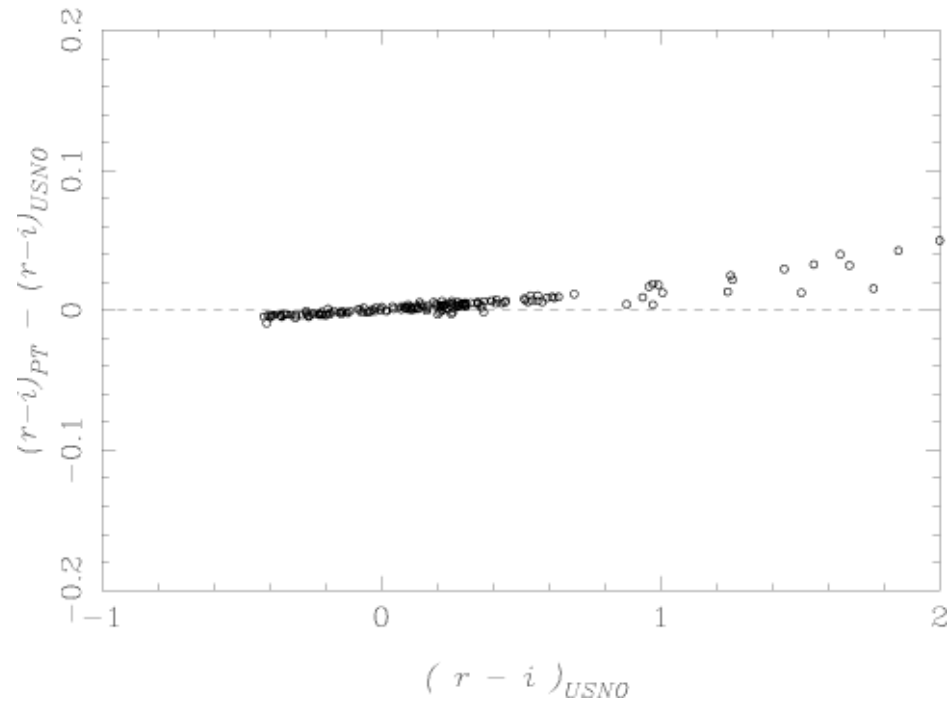


Fig. 14 (c).— The same as Fig.13(a) but for  $r - i$ .

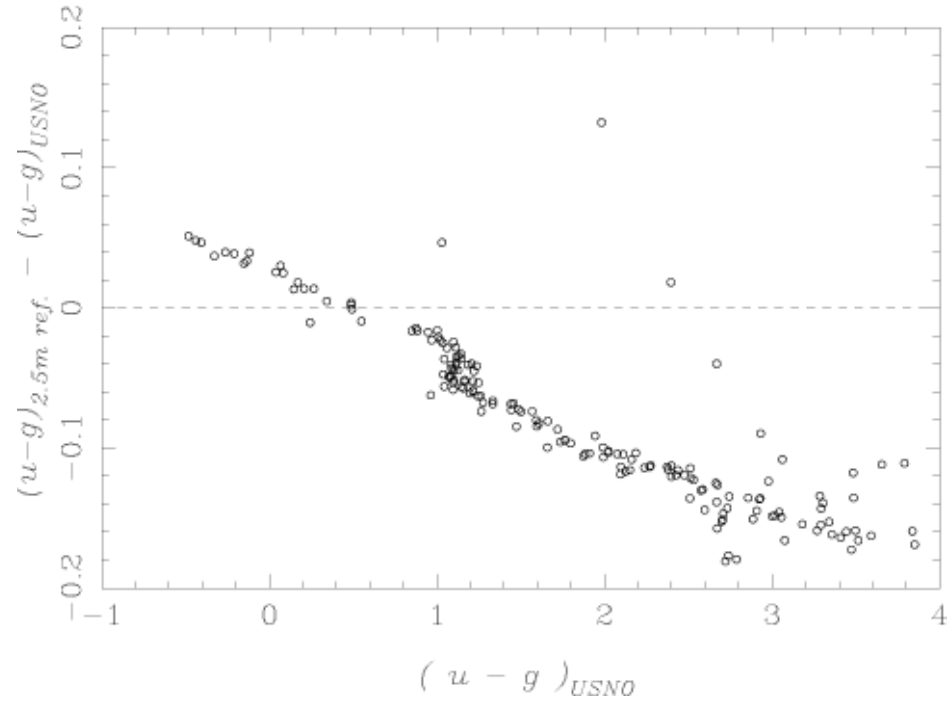


Fig. 15 (a).— Expected offset of  $u-g$  colour between the 2.5m reference and the USNO photometric system,  $\Delta(u-g)_{AB} = (u-g)_{2.5m\ reference} - (u-g)_{USNO}$  plotted as a function of  $u-g$ .

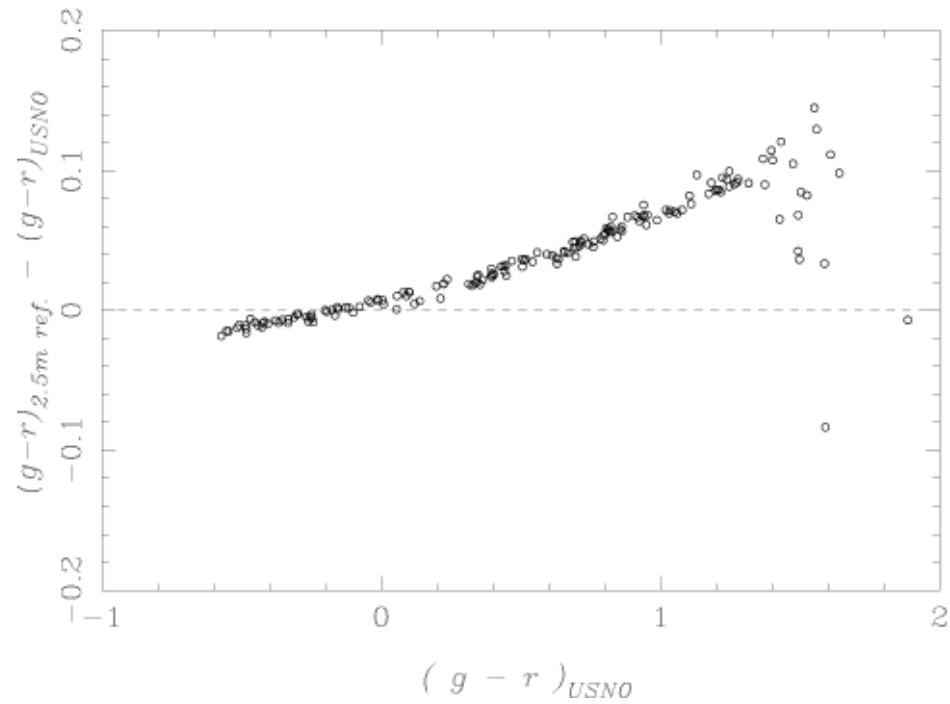


Fig. 15 (b).— The same as Fig.14(a) but for  $g-r$ .

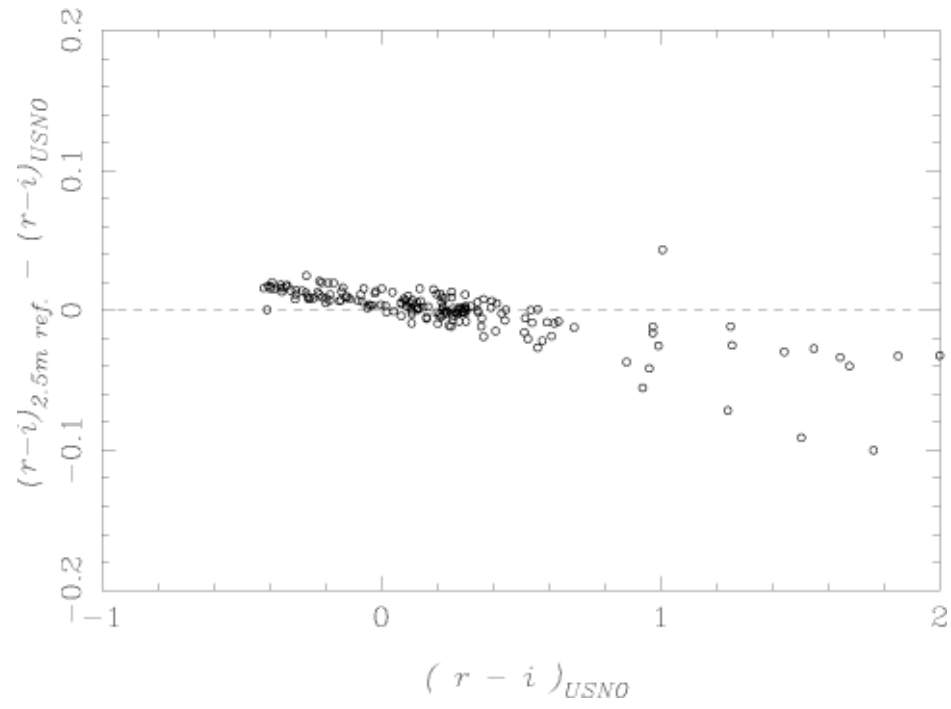


Fig. 15 (c).— The same as Fig.14(a) but for  $r - i$ .

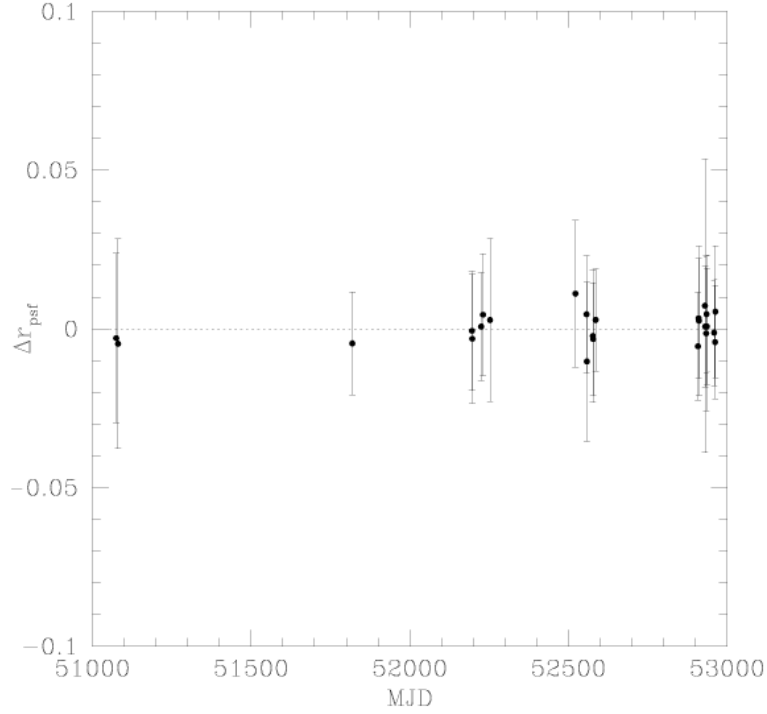


Fig. 16 (a).— Mean of  $r$  brightness of about 600 stars in a patch of 2.5 square degree in Stripe 82 shown as a function of observation epochs from the SDSS catalogue. Error bars mean the variance of the sample.

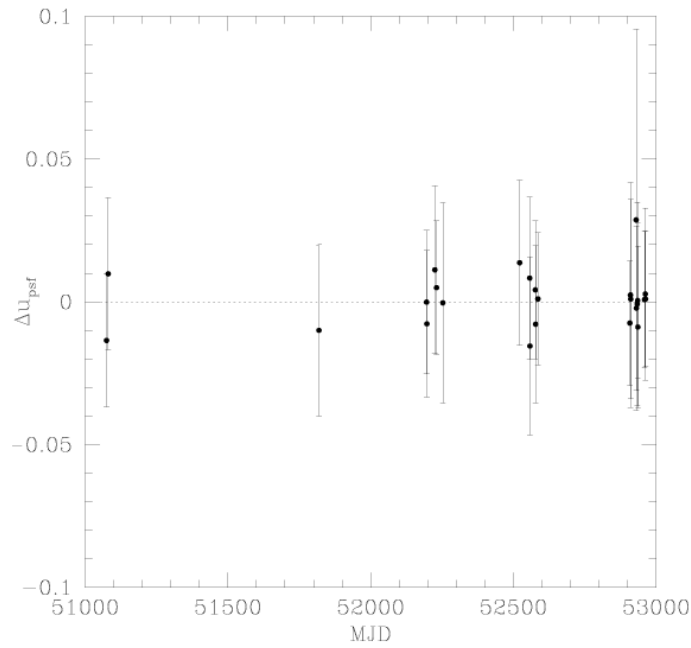


Fig. 16 (b).— Mean of  $u$  brightness using about 200 stars in a patch of 2.5 square degree in Stripe 82 as a function of observation epochs.

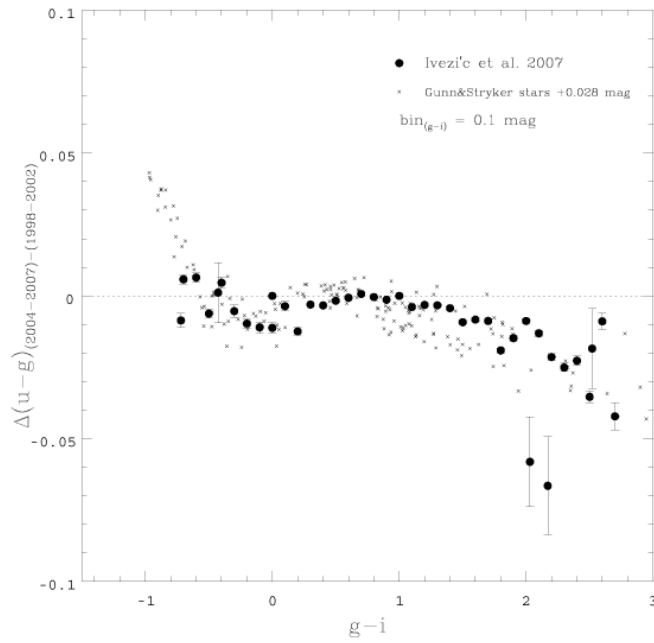


Fig. 17.— The time variation of  $u - g$  colours in repeated photometry at stripe 82 (Ivezić et al. 2007) are shown by filled circles. All the non-variable stars with  $u < 21$  were used. Crosses show colour variation  $\Delta(u - g)$  expected for Gunn-Stryker stars between the 2001 (taken as the zero point) and the 2004 measurements as a function of  $g - i$ . The Error bar is the mean and variance of the data in each colour bin.

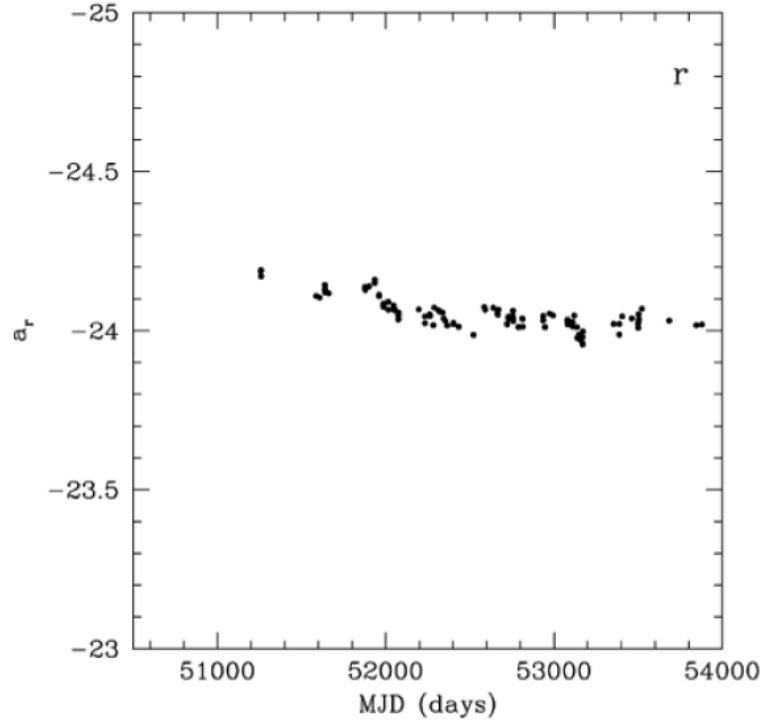


Fig. 18 (a).— Nightly variation of the instrumental photometric zero points of 2.5-m photometry in the  $r$  band.

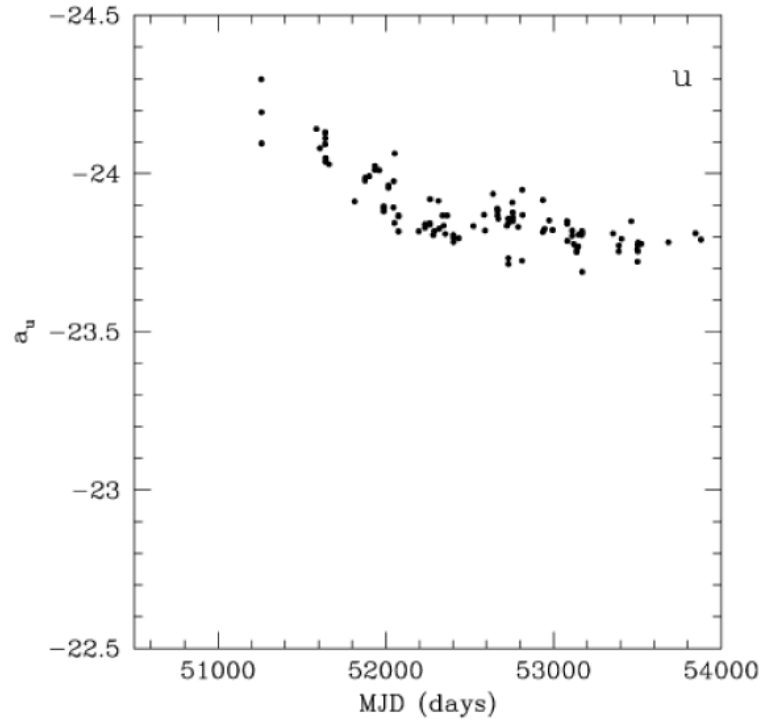


Fig. 18 (b).— Same as (a) but in the  $u$  band.